Chinmo defines the region-specific oncogenic competence in the *Drosophila* central nervous system

Phuong-Khanh Nguyen[1,3], Francesca Froldi[1,2], Owen Marshall[4], Tony D Southall[5], Louise Y Cheng[1,2,3,#]

1. Sir Peter MacCallum Department of Oncology, The University of Melbourne, VIC 3010, Australia
2. Peter MacCallum Cancer Centre, Melbourne, VIC 3000, Australia
3. Department of Anatomy and Physiology, The University of Melbourne, VIC 3010, Australia
4. Menzies Institute for Medical Research Medical Science Precinct, Hobart TAS, Australia
5. Department of Life Sciences, Imperial College London, London, UK.

Corresponding author

Email: louise.cheng@petermac.org

Classification: Biological Sciences / Developmental Biology

Keywords: Dedifferentiation / *Drosophila* / malignancy / terminal differentiation

Abstract

While genetic mutations can promote hyperplastic growth, they do not always result in oncogenic outcomes. We and others have previously identified the transcription factors Nerfin-1 and Lola as inhibitors of dedifferentiation. Here, we investigate how the oncogenic potential of dedifferentiation varies across different neural lineages in the *Drosophila* central nervous system (CNS). We found that Nerfin-1 inactivation causes tumorigenic phenotypes in the central brain (CB) and the ventral nerve cord (VNC) but not the optic lobes (OLs). In contrast, Lola inactivation leads to tumour overgrowth specifically in the OLs. We identify Chinmo, a temporal transcription factor, and its regulation by ecdysone signalling as key determinants of the oncogenic competence in different regions of the brain, influencing the tumorigenic outcome of dedifferentiation. This work provides a fundamental framework to understand how oncogenic competence arises beyond genetic mutations.

Significance statement

In the CNS, the same tumorigenic mutation has been shown cause differential oncogenic outcomes in different regions of the brain. The mechanism underlying this phenomenon remains largely unknown. We have previously demonstrated that malignant brain tumours can be induced via neuronal dedifferentiation in the *Drosophila* CNS. Here, we demonstrate that dedifferentiated neural stem cells drive tumorigenesis in a region-specific manner, accounted for by region-specific expression and regulation of temporal factors by cell-intrinsic and hormonal signals. Together, this work extends our understandings of how brain regionalisation can be a constraint to oncogenesis.

Introduction

Genetic mutations are not the sole determinants of malignant cancer outcomes. In fact, individuals can accumulate mutations with oncogenic potential, yet most are eliminated without leading to malignancy. Oncogenic competence is defined by a combination of genetic mutations, lineage-specific factors, and microenvironmental cues (1). Many brain and central nervous system (CNS) cancers originate from excessively proliferative neural stem-progenitor cells during embryonic development (2, 3). Perturbations in signalling pathways and transcription factors involved in neural development can initiate tumour overgrowth in the CNS (4). Interestingly, distinct oncogenic mutations are associated with specific anatomical regions of the CNS (5–7), suggesting that oncogenic competence is regionally regulated. However, the mechanisms by which region-specific cues influence cancerous transformation remain poorly understood.

The *Drosophila* CNS is a well-established model for studying neurogenesis, cell fate specification, and maintenance during development. In *Drosophila*, neural stem cell-like progenitors, known as neuroblasts (NBs), generate neurons and glia across all regions of the CNS. Here, the CNS is broadly divided into three main regions: the ventral nerve cord (VNC), the central brain (CB), and the optic lobes (OLs) (Fig. 1A). From embryonic to mid-pupal development, NBs undergo a limited number of divisions until their termination, by which the mechanism differs between regions (8–10). In the CB/VNC, NB termination mainly occurs via terminal symmetric division mediated by the homeobox transcription factor Prospero (Pros) (11). Whereas in the optic lobe (OL), medulla NBs undergo termination through a combination of apoptosis, terminal symmetric division, and gliogenic switch (12). Thus, NBs terminate in a region-specific fashion to meet the differential demands of neuronal function during adulthood.

Recent studies have shown that temporal transcription factors (tTFs) and their target genes regulate NB termination in the CB and the VNC. These tTFs are sequentially expressed in NBs as they age, not only specifying distinct neuronal identities in their progeny but also influencing cell cycle speed and the timing of NB termination. For instance, during early larval development, NBs in the CB/VNC express early temporal factors: IGF-II mRNA-binding proteins (Imp) and the BTB-zinc finger transcription factors Chronologically inappropriate morphogenesis (Chinmo) (11, 13, 14). As the animal matures, NBs shift to express late temporal factors, namely Syncrip (Syp) and Broad (Br) (11, 13, 14). Imp and Syp modulate NB proliferation through opposing gradients, with Imp promoting the proliferation whereas Syp driving the termination of NBs (14, 15). Thus, an extended period of Imp expression or inhibition of Syp can prolong NB proliferation (15). Temporal patterning is also observed in the OL medulla progenitors, the NE in which Imp and Chinmo define the early temporal window, while Syp, Br, and Eip93F define the late temporal window (16–18). However, it is unclear if this temporal cascade influences medulla NB termination.

In this study, we investigate how dedifferentiation - triggered by the loss of neuronal cell fate maintenance – can lead to contrasting tumorigenic outcomes. Previously, we and others have shown that neuronal cell fate requires active maintenance by various transcription factors, such as the zinc finger transcription factor Nervous finger 1 (Nerfin-1) and the BTB-zinc finger transcription factor Longitudinals lacking (Lola) (19–22). Failure to maintain the neuronal identity can result in the formation of supernumerary NB that can drive tumour overgrowth. Here, we demonstrate that oncogenic competence of dedifferentiated NBs is region-specific. In the CB and VNC, the loss of Nerfin-1 function leads to malignant tumour overgrowth, with ectopic NBs continuing to proliferate beyond the normal neurogenesis period (21). In contrast, in the OLs, we show that ectopic NBs are eliminated through cell death and differentiation. Unlike Nerfin-1, Lola loss-of-function elicits tumorigenesis in the OL (20). Mechanistically, we identified the early tTF Chinmo as a key regulator of this differential response and that the cell's ability to respond to Chinmo is mediated through ecdysone signalling. As such, increasing Chinmo levels confers oncogenic competence to dedifferentiated NBs induced by Nerfin-1 inactivation in the OL. Conversely, reducing Chinmo levels in those in the CB/VNC or in *lola*$^{-/-}$ clones promote elimination of dedifferentiated NBs. These findings highlight that the differential expression and regulation of oncogenic tTFs such as Chinmo, play a crucial role in determining tumorigenic outcome in response to dedifferentiation triggers. Overall, our study shed light on mechanisms of oncogenic competency and offers insights into how certain regions of the brain are more susceptible to tumorigenesis than others.

Results

nerfin-1 loss-of-function (*nerfin-1*^{159}) causes malignant tumour overgrowth in the CB/VNC but not the OL

We and others have previously reported that *nerfin-1* loss-of-function leads to the dedifferentiation of neurons into ectopic NBs (19, 21, 22). In this study, to investigate region-specific regulation of dedifferentiation, we began by inducing *nerfin-1*^{159}-null mutant (23) loss-of-function MARCM clones at 24 hrs ALH (After Larval Hatching) in all the regions of the larval CNS (CB, VNC, and OLs) (Fig. 1A-C). At wandering L3 stage, control wildtype (WT) MARCM clones in the OL often consist of a few NBs, marked by pan-NB marker Deadpan (Dpn) on the superficial layers and none in the deep layers where neurons reside (Fig. 1D-D'). Whereas *nerfin-1*^{159} clones had many ectopic Dpn^{+} NBs in the deep layers (Fig. 1G-G', J). Similarly, on the superficial layers of the ventral side of the CB (where type I but not type II NBs reside) and the VNC, WT clones consisted of one NB and none in the deep layers that are occupied by neurons (Fig. 1E-F'). In contrast, many ectopic NBs were observed in the deep layers of *nerfin-1*^{159} clones

102 in the CB/VNC (Fig. 1H-J). These data indicate that neurons revert into ectopic NBs in all regions of the
103 CNS upon Nerfin-1 inactivation.

104 In the developing CB/VNC, NBs terminally differentiate at around 24 hrs after pupal formation
105 (APF) (11), and the medulla NBs of the OL terminate between 12-24 hrs APF (12). A key characteristic of
106 malignant tumours is their failure to obey signals to terminally differentiate and their ability to proliferate
107 beyond the normal period of neurogenesis. To examine these characteristics, we analysed the brains at 48
108 hrs APF. In all regions of the brain, no NB persisted in WT clones (Fig. 1K-L', O). However, we observed
109 a discrepancy between the CB/VNC and the OL that contain *nerfin-1*^{159} clones. In the CB/VNC, we found
110 that *nerfin-1*^{159} clones were enriched with ectopic NBs (Fig. 1M-O). Whereas in the OLs, *nerfin-1*^{159} clones
111 became dispersed and devoid of Dpn expression (Fig. 1M-M', O), indicative of neuronal differentiation and
112 migration (24).

113 To ascertain whether *nerfin-1*^{159} NBs undergo proliferation beyond the normal period of
114 neurogenesis, we stained the pupal brains at 48 hrs APF for proliferative NBs marked by Miranda (Mira)
115 and Phospho-Histone 3 (PH3). In all regions of the CNS, WT clones did not exhibit any Mira^{+} PH3^{+}
116 persistent NBs at 48 hrs APF (Fig. 1P-Q'). In contrast, we found that Mira^{+} PH3^{+} NBs were present in
117 *nerfin-1*^{159} clones in the CB/ VNC (Fig. 1R-S', yellow dash lines) but absent in clones in the OL (Fig. 1R-
118 R', arrowheads). Collectively, our results reveal that the same genetic mutation (*nerfin-1*^{159}) can cause
119 differential consequences in a region-specific manner: dedifferentiated NBs drive tumorigenic overgrowth
120 in the CB/VNC but are eliminated in the OL.

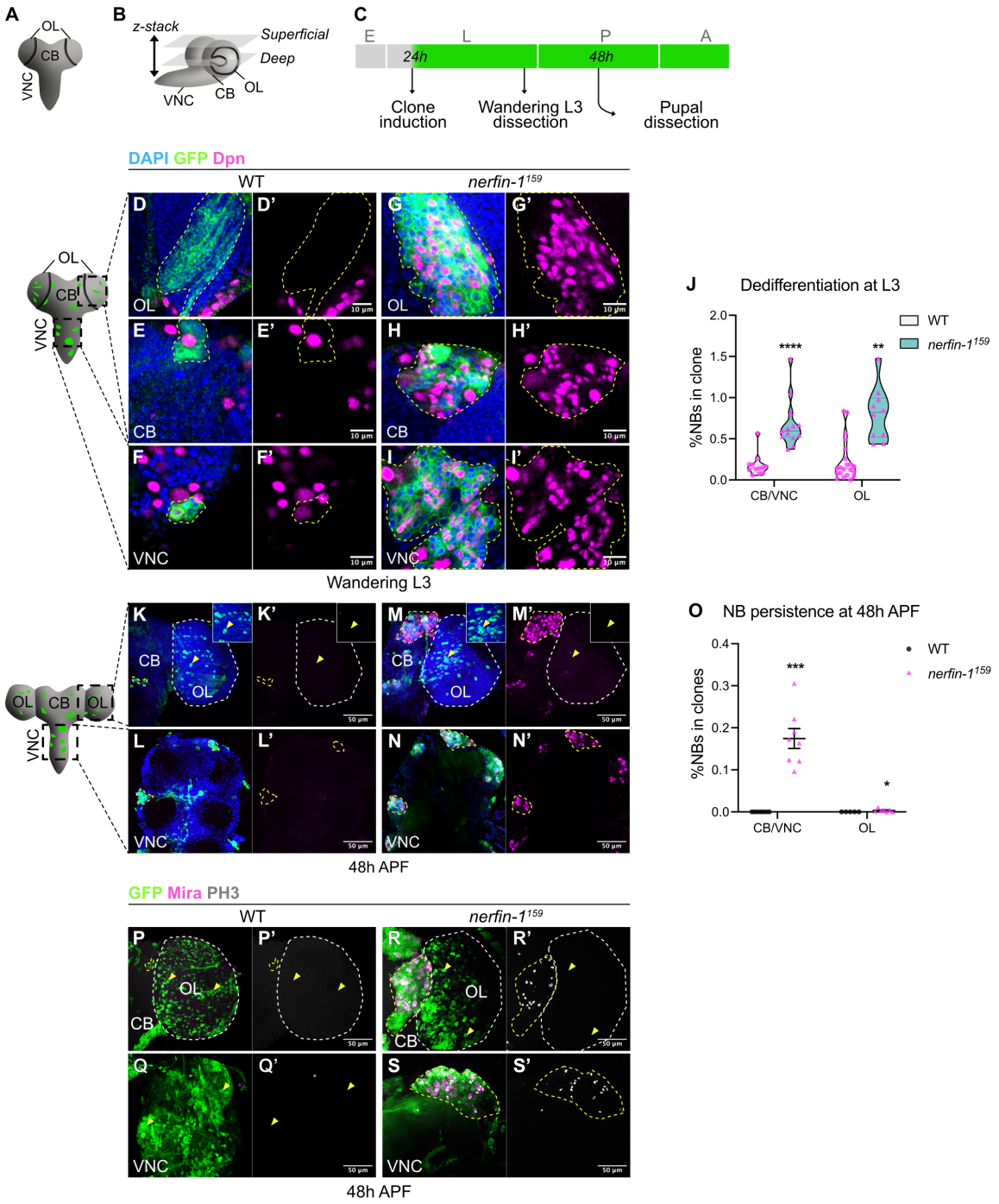

Figure 1: *nerfin-1*^{159} dedifferentiated NBs are selectively eliminated in the pupal OL

A-B. Schematic depicting **(A)** the frontal view and **(B)** the side view of the larval CNS that consists of the central brain (CB), the ventral nerve cord (VNC) and the optic lobes (OLs). Representative confocal images of the larval brain are taken from superficial or deep layers.

C. Schematic summarising our experimental procedure.

D-I'. Single confocal sections in the deep layers of **(D-F')** WT or **(G-I')** *nerfin-1*^{159} clones (dashed lines) in **(D-D', G-G')** the OL, **(E-E', H-H')** CB, and **(F-F', I-I')** VNC at wandering L3 stage. NBs marked by Dpn (magenta), GFP (green), DAPI (blue). Scale bars: 10 µm.

J. Quantification of the percentages of NBs in WT and *nerfin-1*^{159} clones in the CB/VNC and OL at wandering L3 stage. n=12, 10, 9, and 10 clones.

K-N'. Maximum projections of **(K-K', M-M')** the brain lobes (CB and OL, separated by white dash lines) and **(L-L', N-N')** VNC with **(K-L')** WT or **(M-N')** *nerfin-1*^{159} clones (yellow dash lines) at 48h APF. DAPI (blue), GFP (green), Dpn (magenta). Arrowheads indicate GFP^{+} cells. Scale bars: 10 µm.

O. Quantification of the percentages of NBs in WT and *nerfin-1*^{159} clones in the CB/VNC and OL at 48h APF. n=7, 8, 5, and 7.

P-S'. Maximum projections of **(P-P', R-R')** the brain lobes (CB and OL, separated by white dash lines) and **(Q-Q', S-S')** VNC with **(P-Q')** WT or **(R-S')** *nerfin-1*^{159} clones at 48h APF. Arrowheads indicate GFP^{+} cells. Yellow dash lines indicate tumour formation in the CB/VNC. Mature NBs are marked by Miranda (Mira, magenta), mitotic cells are marked by Phospho-Histone 3 (PH3, grey), GFP (green). Scale bars: 50 µm.

Data information: Data are represented as mean ± SEM. *p*-values were obtained using Mann-Whitney test. ****$p < 0.0001$, ***$p < 0.001$, **$p < 0.005$, *$p < 0.05$.

nerfin-1^{159} dedifferentiated NBs in the OL are eliminated via a combination of Pros-mediated differentiation and apoptosis-mediated cell death

To test how *nerfin-1*^{159} dedifferentiated NBs become eliminated in the pupal OL, we examined whether these NBs undergo differentiation or a gliogenic switch – mechanisms responsible for WT OL NB termination (12). First, we assayed for the expression of the neuronal marker Elav and glial marker Repo in *nerfin-1*^{159} clones at 48 hrs APF. We found that *nerfin-1*^{159} clones contained Elav^{+} neurons (Fig. 2A-B'', cyan arrowheads) and Repo^{+} glial cells (Fig. 2A-B'', magenta arrowheads) in both pupal OL and VNC. Additionally, the rate of neuronal differentiation (percentage of Elav^{+} volume per region of interest, see Material and Methods) was significantly higher in the OL than the VNC at 48 hrs APF (Fig. 2C). The terminal differentiation of WT NBs via symmetric division is mediated by the homeobox transcription factor Pros (11, 12). At 24 hrs APF, we found that *nerfin-1*^{159} NBs in both the OL and VNC expressed low levels of Pros (Fig. 2D-E'', arrowheads), suggesting that the elimination of these ectopic NBs requires terminal differentiation. To address this, we knocked down Pros in *nerfin-1*^{159} clones. At wandering L3 stage, ectopic NBs were found in both *pros*^{RNAi} and *pros*^{RNAi}*;nerfin-1*^{159} clones in the deep layers of the OLs (Fig. 2F-H). By 48 hrs APF, *pros*^{RNAi}*;nerfin-1*^{159} clones exhibited significantly increased NB persistence compared to *nerfin-1*^{159} or *pros*^{RNAi} clones (Fig. 2I-K', M). This suggests that Pros-mediated terminal differentiation contributes to the elimination of *nerfin-1*^{159} dedifferentiated NBs in the pupal OL. To elucidate whether the gliogenic switch also contributes to the elimination of *nerfin-1*^{159} dedifferentiated NBs, we knocked down the glial cell fate determinant Glial-cell-missing (Gcm) by RNAi. However, this manipulation did not significantly increase the persistence of ectopic NBs at 48 hrs APF (Fig. 2L-L', N).

164 Hence, an acquisition of the glial cell fate does not substantial contribute to the elimination of *nerfin-1*^{159}
165 dedifferentiated NBs in the pupal OL.

166 A subset of NBs in the developing OL terminates via apoptosis-mediated cell death during early
167 pupal development (12). At wandering L3 stage, we found that some dedifferentiated NBs in *nerfin-1*^{159}
168 clones expressed the apoptotic marker Caspase-1 (Dcp-1) (Fig. S1A-A', arrowheads). To address if
169 apoptosis is required for the elimination of *nerfin-1*^{159} dedifferentiated NBs, we inhibited apoptosis by
170 overexpressing the apoptotic inhibitor p35 in *nerfin-1*^{159} clones. This perturbation resulted in the elimination
171 of Dcp-1 expression in the NBs at wandering L3 stage, indicating that apoptosis was suppressed (Fig. S1B-
172 B'). This was accompanied by a small increase in the NB persistence in *nerfin-1*^{159} clones at 48 hrs APF
173 (fig. S1C-E). However, most of the *UAS-p35;nerfin-1*^{159} cells in the OLs were devoid of Dpn (Fig. S1D-
174 D', white arrowheads). We found that many *UAS-p35;nerfin-1*^{159} cells in the pupal OL expressed either
175 Elav or Repo (Fig. S1F-F''), suggesting that the cells that do not die may still undergo terminal
176 differentiation or acquire a glial cell fate. Together, our data suggest that the elimination of *nerfin-1*^{159}
177 dedifferentiated NBs in the pupal OL involves a combination of Pros-mediated terminal differentiation and
178 apoptosis.

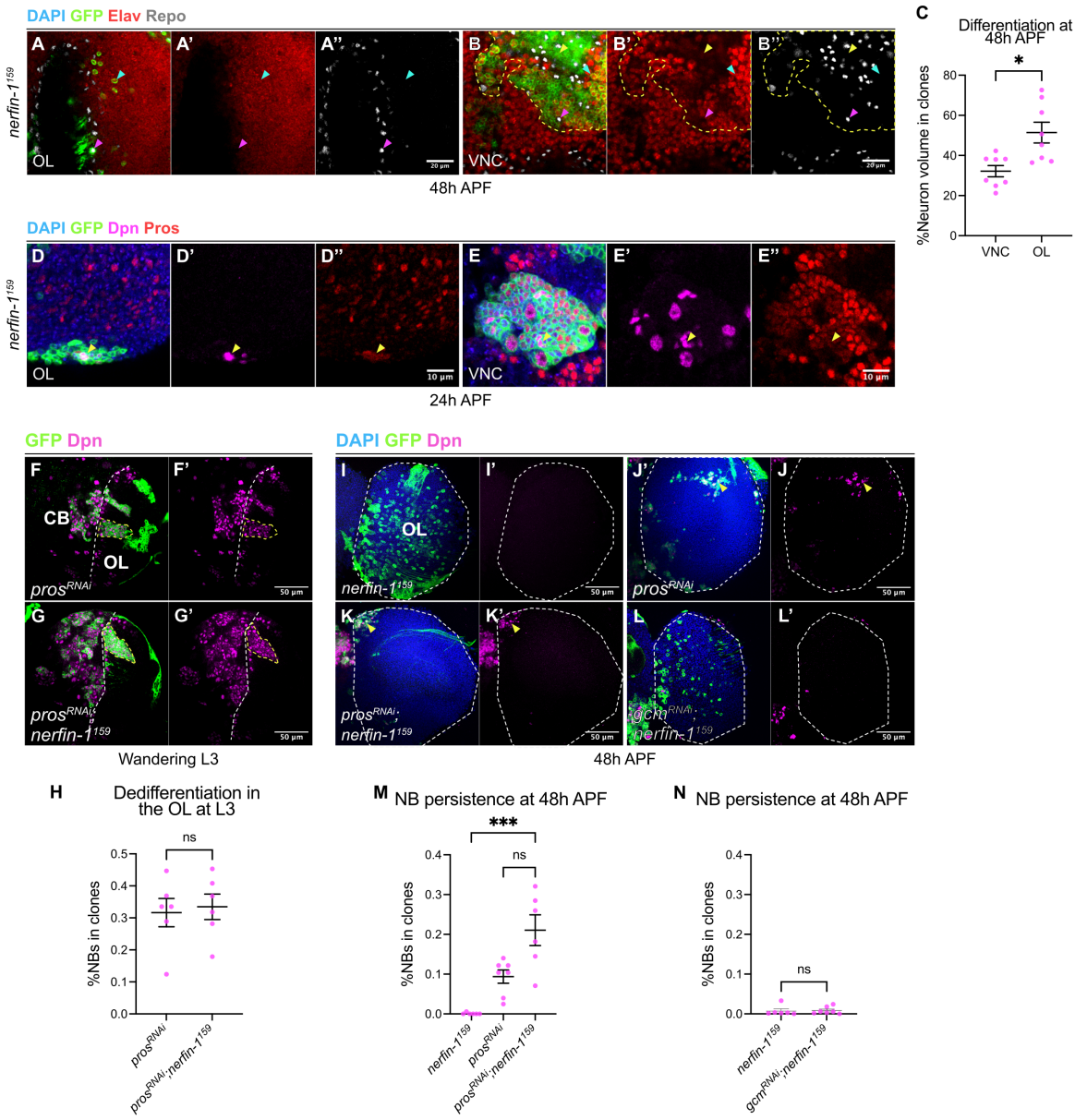

Figure 2: *nerfin-1^{159}* dedifferentiated NBs in the OL are eliminated via Pros-mediated terminal differentiation during pupal development

A-B". Single confocal sections of *nerfin-1^{159}* clones in **(A-A")** the OL and **(B-B")** the VNC at 48h APF. GFP (green), Elav (red), Repo (grey). In the VNC, yellow dash lines outline the mutant clone. Yellow arrowhead indicates Elav^{-}Repo^{-} mutant cell. Cyan and magenta arrowheads indicate Elav^{+}Repo^{-} and Elav^{-}Repo^{+} mutant cells, respectively. Scale bars: 20 µm.

C. Quantification of the percentages of the volume of neurons in *nerfin-1^{159}* clones in the OL and the VNC at 48h APF. VNC: n=8, and 8.

D-E". Single confocal sections of *nerfin-1^{159}* clones in **(D-D")** the OL and **(E-E")** the VNC at 24h APF. DAPI (blue), GFP (green), Dpn (magenta), Pros (red). Scale bars: 10 µm.

F-G'. Single confocal sections in the deep layers of the brain lobes at wandering L3 stage with **(F-F')** *pros*^{RNAi} and **(G-G')** *pros*^{RNAi}*;nerfin-1*^{159} clones (yellow dash lines). GFP (green), Dpn (magenta). White dash lines outline the CB/OL borders. Scale bars: 50 µm.

H. Quantification NB percentages in *pros*^{RNAi} and *pros*^{RNAi}*;nerfin-1*^{159} clones in the OL at wandering L3 stage. n=6, and 6 clones.

I-L'. Maximum projections of the OL (dash lines) at 48h APF with **(I-I')** *nerfin-1*^{159}, **(J-J')** *pros*^{RNAi}, **(K-K')** *pros*^{RNAi}*;nerfin-1*^{159} and **(L-L')** *gcm*^{RNAi}*;nerfin-1*^{159} clones. Arrowheads indicate ectopic NBs. DAPI (blue), GFP (green), Dpn (magenta). Scale bars: 50 µm.

M. Quantifications of NB percentages in *nerfin-1*^{159}, *pros*^{RNAi}, and *pros*^{RNAi}*;nerfin-1*^{159} clones in the OLs at 48h APF. n=6, 6, and 7.

N. Quantifications of the percentages of NBs in *nerfin-1*^{159} and *gcm*^{RNAi}*;nerfin-1*^{159} clones in the OLs at 48h APF. n=6, and 7.

Data information: Data are represented as mean ± SEM. *p*-values were obtained using Mann-Whitney test and Kruskal-Wallis test with Dunn's test to correct for multiple comparisons. ****$p < 0.0001$, *$p < 0.05$.

The elimination *of nerfin-1*^{159} dedifferentiated NBs in the pupal OL occurs independently of Myc

In the VNC, we previously showed that *nerfin-1*^{159}-induced neuronal dedifferentiation is dependent on the expression of the growth regulator Myc (21). Interestingly, our immunostaining showed that Myc was expressed in *nerfin-1*^{159} clones in the CB and VNC but not in the OL at wandering L3 stage (Fig. S1G-H'). Hence, it is plausible the elimination of *nerfin-1*^{159} dedifferentiated NBs in the pupal OL is caused by the lack of Myc. To test this hypothesis, we overexpressed Myc in *nerfin-1*^{159} clones. While this manipulation was sufficient to increase Myc levels in *nerfin-1*^{159} clones in the OL, it was not sufficient to promote the persistence of ectopic NBs at 48 hrs APF (Fig. S1E, I-J'').

The elimination *of nerfin-1*^{159} dedifferentiated NBs in the pupal OL is due to the absence of the oncogenic temporal factor Chinmo

In the VNC, the malignant tumour competency is determined by the expression of the oncogenic tTF Chinmo, such that cells generated during the Imp^{+}Chinmo^{+} window are susceptible to malignant tumour overgrowth (25, 26). Whereas late-born cells from the Syp^{+}Br^{+} temporal window have the propensity to undergo terminal differentiation. To investigate if Chinmo is involved in the elimination of *nerfin-1*^{159} dedifferentiated NBs in the pupal OL, we first examined Chinmo expression in *nerfin-1*^{159} clones at wandering L3 stage. Consistent with previous reports (26), we found that Chinmo was expressed in many WT neurons as well as *nerfin-1*^{159} dedifferentiated NBs in the CB and VNC (Fig. 3A-B'' and Fig. S2A-A''). In contrast, the majority of neurons and *nerfin-1*^{159} dedifferentiated NBs in the OL did not express Chinmo (Fig. 3C-C'' and Fig. S2B-B'').

To test whether Chinmo is functionally required to promote the persistence of dedifferentiated NBs in the CB/VNC, we expressed *chinmo*^{RNAi} (see Materials and methods for details of RNAi construction) in *nerfin-1*^{159} clones. At wandering L3 stage, the expression of *chinmo*^{RNAi} effectively reduced Chinmo levels in *nerfin-1*^{159} clones in the VNC (Fig. 3D-E''). At 48 hrs APF, *chinmo*^{RNAi}*;nerfin-1*^{159} clones significantly reduced NB persistence compared to *nerfin-1*^{159} clones (Fig. 3F-H). Hence, Chinmo is required to promote tumorigenesis of *nerfin-1*^{159} dedifferentiated NBs in the pupal CB/VNC.

Next, we sought to address whether the absence of Chinmo accounts for the elimination of *nerfin-1*^{159} dedifferentiated NBs in the pupal OL. To do so, we overexpressed a full-length version of *chinmo* (*chinmo*^{FL}) (27) in *nerfin-1*^{RNAi} flip-out clones. By 24 hrs APF, *nerfin-1*^{RNAi}*;mCherry*^{RNAi} control clones in the OL were devoid of Dpn and cells were dispersed across the OLs (Fig. 3I-I'). In contrast, *nerfin-1*^{RNAi};*chinmo*^{FL} clones contained persistent ectopic NBs (Fig. 3J-K). From mid-larval stages, medulla NBs located on the cortical surface are generated from a pseudostratified neuroepithelium (NE) of the OL named the NE-NB transition (28, 29). Importantly, Chinmo was previously shown to play a critical role in regulating the NE-NB transition (17). In early larval development, Chinmo is expressed in the NE to promote NE self-renewal whereas from mid-larval stages, Chinmo is downregulated, allowing NE differentiation into NBs. Thus, the overexpression of Chinmo in the NE can result in a delayed NE-NB transition which can subsequently delays NB termination (17). To overexpress Chinmo in a subset of medulla NB (and not NE), we utilised *tub-GAL80*^{ts};*eyR16F10-GAL4* (12) to drive the expression of *chinmo*^{FL} temporally from early L3 . At wandering L3 stage, ectopic NBs were found in the deep layers of the medulla upon the induction of *nerfin-1*^{RNAi} (Fig. S2C-E'). At 24 hrs APF, *nerfin-1*^{RNAi}*;mCherry*^{RNAi} and *lacZ*^{RNAi}*;mCherry*^{RNAi} OLs exhibited no persistent NBs (fig. S2F-G', I). In contrast, many ectopic NBs were observed in the OLs upon the misexpression of *nerfin-1*^{RNAi}*;UAS-chinmo*^{FL} (Fig. S2H-I). Altogether, our data suggest that Chinmo is sufficient to prevent the elimination of *nerfin-1* loss-of-function NBs in the pupal OL.

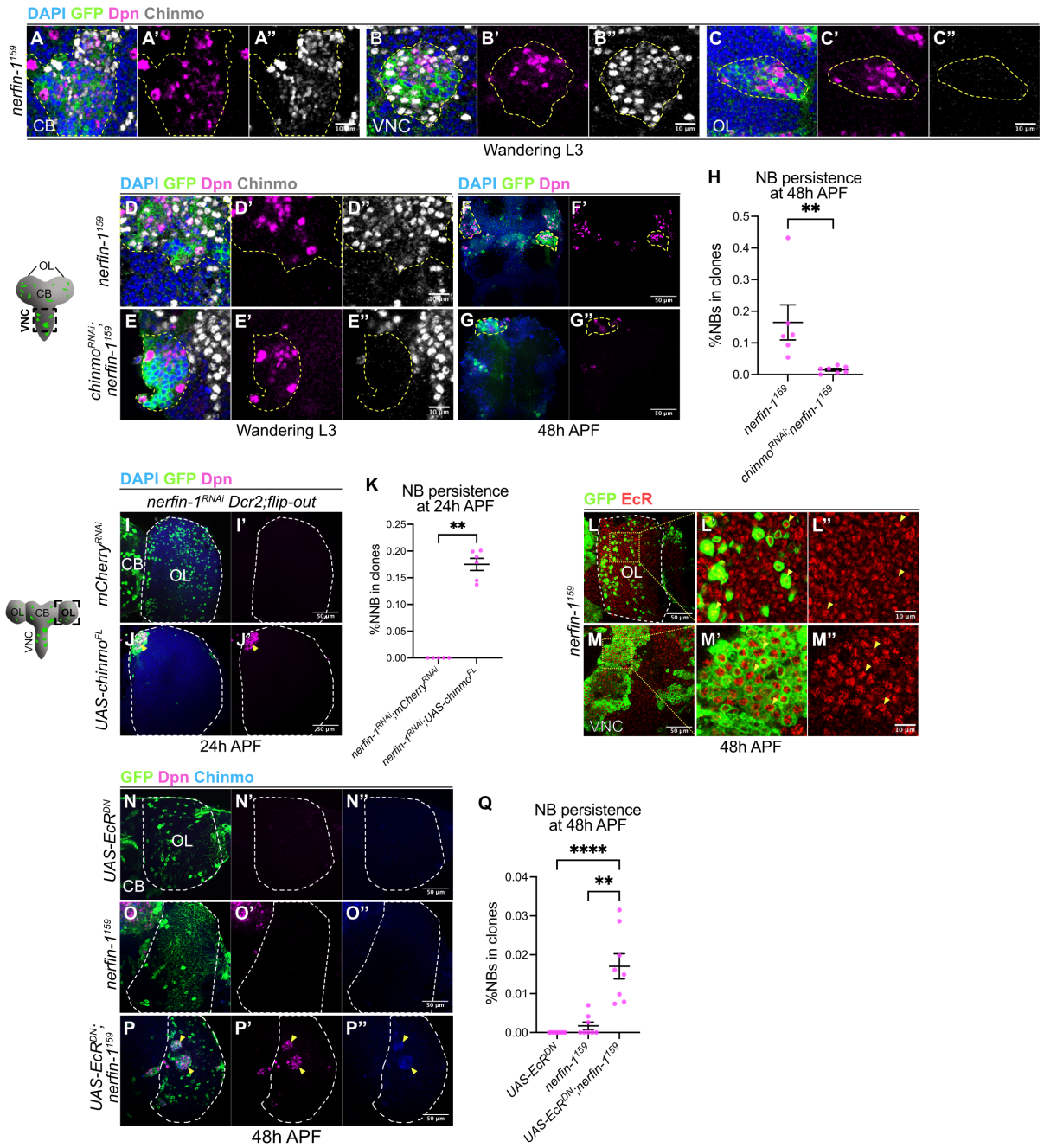

Figure 3: Chinmo promotes the persistence of *nerfin-1*^{159} ectopic NBs in the pupal CNS

A-C". Single confocal sections of *nerfin-1*^{159} clones (dash lines) in **(A-A")** the CB, **(B-B")** VNC and **(C-C")** OL at wandering L3 stage. DAPI (blue), GFP (green), Dpn (magenta), Chinmo (grey). Scale bars: 10 µm.

D-E" Single confocal sections of **(D-D")** *nerfin-1*^{159} and **(E-E")** *chinmo*^{RNAi};*nerfin-1*^{159} clones (dash lines) in the VNC at wandering L3 stage. DAPI (blue), GFP (green), Dpn (magenta), Chinmo (grey). Scale bars: 10 µm.

F-G'. Maximum projections of the VNC with **(F-F')** *nerfin-1*^{159} and **(G-G')** *chinmo*^{RNAi};*nerfin-1*^{159} clones (dash lines) at 48h APF. DAPI (blue), GFP (green), Dpn (magenta). Scale bars: 50 µm.

H. Quantification of the percentages of NBs in *nerfin-1*^{159} and *chinmo*^{RNAi}*;nerfin-1*^{159} clones in the VNC at 48h APF. n=6, and 7.

I-J'. Maximum projections of the OLs (dash lines) at 24h APF with **(I-I')** *nerfin-1*^{RNAi}*;mCherry*^{RNAi} and **(J-J')** *nerfin-1*^{RNAi}*;UAS-chinmo*^{FL} flip-out clones. Arrowheads indicate persistent ectopic NBs. DAPI (blue), GFP (green), Dpn (magenta). Scale bars: 50 µm.

K. Quantification of the percentages of NBs in *nerfin-1*^{RNAi}*;mCherry*^{RNAi} and *nerfin-1*^{RNAi}*;UAS-chinmo*^{FL} flip-out clones in the OLs at 24h APF. n=5, and 6.

L-M". Left panels: single confocal section of the **(L-L")** OL (dash lines) and **(M-M")** VNC at 48h APF with *nerfin-1*^{159} clones (arrowheads). Right panels are boxed area in left panels. GFP (green), EcR (red). Scale bars: 50 and 10 µm.

N-P" Single confocal sections of the OLs (dash lines) at 48h APF with **(N-N")** *UAS-EcR*^{DN}, **(O-O")** *nerfin-1*^{159} and **(P-P")** *UAS-EcR*^{DN};*nerfin-1*^{159} clones. Arrowheads indicate persistent ectopic Chinmo^{+} NBs. GFP (green), Dpn (magenta), Chinmo (blue). Scale bars: 50 µm.

Q. Quantification of the percentages of NBs in *UAS-EcR*^{DN}*, nerfin-1*^{159}, and *UAS-EcR*^{DN}*;nerfin-1*^{159} clones in the OLs at 48h APF. n=8, 8, and 8.

Data information: Data are represented as mean ± SEM. *p*-values were obtained using Mann-Whitney test and Kruskal-Wallis test with Dunn's test to correct for multiple comparisons. ****$p < 0.0001$, **$p < 0.005$.

Chinmo is repressed by ecdysone signalling in *nerfin-1*^{159} clones in the OL

We next investigated how Chinmo expression is regulated in *nerfin-1*^{159} clones in the OL. In the developing OL medulla, Chinmo has been shown to be expressed from early to mid-larval stages (16, 17). As *nerfin-1*^{159} clones in the larval OL were devoid of Chinmo expression (Fig. 3C-C''), we next investigated how Chinmo expression is repressed, and whether this is regulated by transcriptional or post-transcriptional mechanisms. We first assessed the expression of *chinmo*-lacZ transcriptional reporter in *nerfin-1*^{159} clones in the CB, VNC and the OL at wandering L3 stage. In the CB and VNC, *chinmo*-lacZ was expressed in *nerfin-1*^{159} clones (Fig. S2J-K''). On the contrary, *chinmo*-lacZ was absent in *nerfin-1*^{159} clones in the OL (Fig. S2J''), indicating that *chinmo* is transcriptionally silenced in *nerfin-1*^{159} clones the OL but not the CB/VNC. We then also tested if *chinmo* can be post-transcriptionally controlled in *nerfin-1*^{159} clones. To do so, we utilised a reporter in which the mCherry coding sequence is flanked by the 5' and 3' UTRs of *chinmo* (*UAS-mCherry-chinmo*^{UTRs}) (17). If *chinmo* is regulated post-transcriptionally, it is expected that clones would not express mCherry. However, we found that similar to WT clones *nerfin-1*^{RNAi} flip-out clones expressed mCherry (Fig. S2L-M'', dash lines), indicating that Chinmo expression is regulated via transcriptional rather than post-transcriptional mechanisms.

Ecdysone is a steroid hormone and a central regulator of developmental transitions in insects including *Drosophila* (30). In the WT CNS, it has been previously shown that ecdysone signalling at the critical weight (mid-L3 stage) is required to repress Chinmo transcription specifically in the OL but not the

294 CB/VNC (17). Therefore, it is plausible that ecdysone signalling inhibits Chinmo expression in *nerfin-1*^{159}
295 dedifferentiated NBs in the OL. We found that Ecdysone Receptor (EcR) was expressed in *nerfin-1*^{159} clones
296 at a similar level to the surrounding WT cells at 48 hrs APF in the OL and VNC (Fig. 3L-M'', arrowheads),
297 suggesting that *nerfin-1*^{159} clones may be responsive to ecdysone signals. To inhibit ecdysone signalling,
298 we expressed a dominant negative form of EcR (EcR^{DN}) (31) in *nerfin-1*^{159} clones and assayed for Chinmo
299 expression at 48 hrs APF. While *UAS-EcR*^{DN} expression alone was not sufficient to upregulate Chinmo, nor
300 promote the persistence of NBs (Fig. 3N-N'',Q), *UAS-EcR*^{DN} expression in *nerfin-1*^{159} clones caused
301 Chinmo to be upregulated and resulted in increased NB persistence in the OL (Fig. 3O-Q). These data
302 suggest that ecdysone signalling is necessary for Chinmo silencing in *nerfin-1*^{159} clones in the pupal OL,
303 causing the dedifferentiated NBs to lose tumorigenicity and differentiate. It is of note that *nerfin-1*^{159} clones
304 in the VNC also expressed EcR (Fig. 3M-M''). Nevertheless, because *nerfin-1*^{159} dedifferentiated NBs
305 persist in the pupal CB/VNC, it is likely that they do not respond to ecdysone signals.

306 We also examined if known post-transcriptional regulators of Chinmo such as the RNA-binding
307 protein Imp (32) or the microRNA *let-7* (33) can upregulate Chinmo expression in *nerfin-1*^{159} clones and
308 thereby, promote ectopic NB persistence in the pupal OL. At 24 hrs APF, we found that the overexpression
309 of Imp in *nerfin-1*^{159} clones was able to downregulate its antagonist Syp but was however not sufficient to
310 upregulate Chinmo expression (Fig. S2N-O'''). Additionally, by 48 hrs APF, the percentages of persistent
311 NBs in *UAS-Imp;;nerfin-1*^{159} clones were comparable to that of *nerfin-1*^{159} clones (Fig. S2P). As such, Imp
312 is not sufficient to upregulate Chinmo expression or promote tumour overgrowth in the OL. To functionally
313 test the role of *let-7*, we misexpressed *let-7*^{sponge} in *nerfin-1*^{159} clones and assayed for ectopic NBs in the OL
314 at 48 hrs APF. Similar to Imp overexpression, no NB persisted in both *let-7*^{sponge}*;nerfin-1*^{159} (n=6/6 lobes)
315 and *nerfin-1*^{159} clones (n=3/3 lobes) (Fig. S2Q-R'), suggesting that *let-7* is unable to promote
316 dedifferentiated NBs to persist in the pupal OL. Altogether, our results are consistent with the notion that
317 *chinmo* is transcriptionally silenced by ecdysone signalling between larval-pupal development in *nerfin-*
318 *1*^{159} clones in the OL. Hence, altering post-transcriptional modulators of Chinmo is not sufficient to prevent
319 the elimination of *nerfin-1*^{159} dedifferentiated NBs.

320

321 **Lola and Nerfin-1 have different expression patterns and regulate different gene sets in the**
322 **developing OL medulla**

323 *lola* loss-of-function (*lola*^{E76} – a null mutation where all Lola isoforms are deleted) (Goeke et al., 2003)
324 causes neuronal dedifferentiation and consequently, tumour formation specifically in the adult OL (Southall
325 et al., 2014). Indeed, we observed ectopic NB formation in *lola*^{E76} clones in the deep layers of the OL at

326 wandering L3 stage (Fig. 4A-B), indicating neuronal dedifferentiation. At 48 hrs APF, unlike WT clones in
327 which NBs already terminated, *lola*^{E76} clones in the OL consisted of multiple ectopic Dpn^{+} NBs (Fig. 4C-
328 D) as well as many Mira^{+}PH3^{+} NBs (Fig. 4E-F). Therefore, it is likely that these NBs were capable of
329 proliferation beyond the normal period of neurogenesis. Notably, we found that some cells within *lola*^{E76}
330 clones were able to undergo differentiation, as indicated by the presence of neuronal marker Elav and glial
331 marker Repo (Fig. S3A-A'''). Furthermore, nuclear expression of Pros was detected in *lola*^{E76} NBs similar
332 to WT cells in the OL at 24 hrs APF (Fig. S1B-C''), suggesting that *lola*^{E76} ectopic NBs can undergo Pros-
333 mediated terminal symmetric division. Together, these data suggest that beyond region-specific
334 mechanisms, the ability to form tumours is also determined by the nature of the genetic mutations; while
335 *nerfin-1*^{159} dedifferentiated NBs are eliminated, *lola*^{E76} dedifferentiated NBs remain proliferative to initiate
336 tumorigenesis in the pupal OL.

337 As tumours generated via the loss-of-function of *nerfin-1* and *lola* caused distinct outcomes in the
338 OL, we hypothesized that Nerfin-1 and Lola regulate different sets of target genes during medulla
339 neurogenesis. To test this hypothesis, we first characterised the expression pattern of Nerfin-1 and Lola
340 using their respective GFP reporters in the OL at wandering L3 stage. Upon NE-NB transition, each NB
341 divides asymmetrically to self-renew and generate GMCs, which in turn divide once to produce medulla
342 neurons (28, 29) (Fig. 4G). The birth order of neurogenesis dictates that the latest born neurons occupying
343 the most superficial position close to NBs and GMCs, and the earliest born neurons occupying the deepest
344 layer. We stained the larval brains for PatJ to mark the apical membrane of NE cells and Dpn to mark NBs.
345 For Lola, we used a GFP against Lola isoform I (Lola.I::GFP) which was previously shown to be expressed
346 in the NBs and neurons of the larval OLs (35). We observed that Lola.I::GFP was expressed in the nuclei
347 of PatJ^{+} NE cells (Fig. 4H-I''', yellow dash lines) and Dpn^{+} NBs (Fig. 4H-I''', arrowheads). Conversely,
348 Nerfin-1::GFP was not expressed in the NE and the majority of the NBs (Fig. 4J-K'''). Together, these data
349 suggest that Lola and Nerfin-1 are likely required to function in different cell types in the OL.

350 To explore target genes downstream of Lola and Nerfin-1, we performed RNA-sequencing and
351 compared the transcriptional profiles of *lola*^{E76}, *nerfin-1*^{159}, and WT clones from the OLs of wandering L3
352 larva (Fig. S3D). Our differential expression analyses (adjusted p-value<0.05; fold-change, FC>1.5)
353 revealed 94 differentially expressed genes, including 65 upregulated and 29 downregulated genes in *lola*^{E76}
354 compared to WT clones. Between *nerfin-1*^{159} and WT clones, there were 164 differentially expressed genes,
355 including 80 upregulated and 82 downregulated genes. Notably, only 11 genes were shared between *lola*^{E76}
356 versus WT and *nerfin-1*^{159} versus WT comparisons (Fig. S3E). Intriguingly, between *lola*^{E76} and WT clones,
357 gene ontology (GO) enrichment for upregulated genes included terms involved in the digestive tract and
358 muscle development (Fig. S3F). These unexpected results suggest that Lola may play a role in suppressing

359 non-CNS genes to ensure the faithfulness of neural identity. Whereas GO enrichment for downregulated
360 genes included synaptic transmission and membrane potential (Fig. S3F), indicating that Lola promotes
361 genes required for neuronal maturation. GO terms enriched for genes upregulated in *nerfin-1*^{159} clones
362 included NB division and proliferation (Fig. S3G). Conversely, GO terms enriched for genes downregulated
363 included terms involved in regulation of synaptic transmission and membrane potential (Fig. S3G).
364 Therefore, Nerfin-1 appears to govern neuronal cell fate maintenance by inhibiting self-renewal and
365 proliferation genes while promoting neuronal maturation. Collectively, our data suggest that Lola and
366 Nerfin-1 have different expression patterns and target different sets of genes with minimal overlap in the
367 developing medulla.

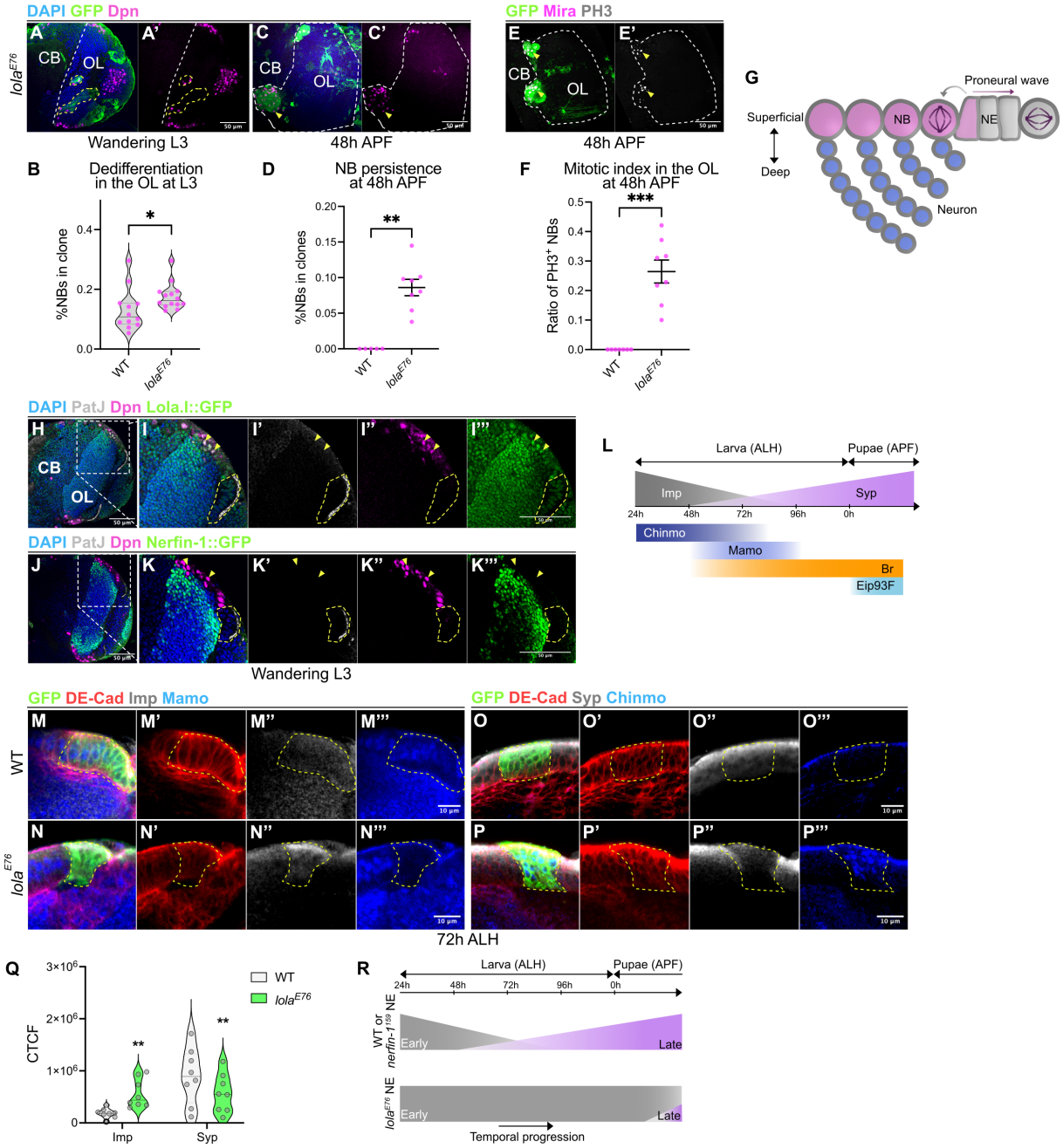

Figure 4: Lola promotes temporal progression of the larval NE

A-A'. Single section of the late L3 OL (deep layer) with *lola*^{E76} clones (dash lines). DAPI (blue), GFP (green), Dpn (magenta). Scale bars: 50 µm.

B-B'. Quantification of NB percentages in WT and *lola*^{E76} clones in the late L3 OLs. n=12 and 14 clones.

C-C'. Maximum projections of the OL (dash lines) at 48h APF with *lola*^{E76} clones (arrowheads). DAPI (blue), GFP (green), Dpn (magenta). Scale bars: 50 µm.

D. Quantification of NB percentages in WT and *lola*^{E76} clones in the OLs at 48h APF. n=5 and 8.

E-E'. Maximum projections of the OL (dash lines) at 48h APF with *lola*^{E76} clones (arrowheads). GFP (green), Mira (magenta), PH3 (grey). Scale bars: 50 µm.

F. Quantification of mitotic NB percentages in WT and *lola*^{E76} clones in the OLs at 48h APF. n=7 and 8.

G. Schematic depicting the larval OL medulla.

H-K''' Single sections of late L3 brain lobes expressing **(H-I''')** Lola.I::GFP and **(J-K''')** Nerfin-1::GFP. **(I-I''')** and **(K-K''')** are boxed areas in **(H)** and **(J)**, respectively. DAPI (blue), PatJ (grey) marks the NE (dash lines), Dpn (magenta), GFP (green). Arrowheads indicate NBs. Scale bars: 50 and 10 µm.

L. Schematic depicting temporal series in the NE.

M-P'''. Single section of superficial layer **(M-M''', O-O''')** WT and **(N-N''', P-P''')** with *lola*^{E76} clones (dash lines) at 72h ALH. GFP (green), DE-Cad (red) marks the NE. **(M-N''')** Imp (grey), Mamo (blue). **(O-P''')** Syp (grey), Chinmo (blue). Scale bars: 10 µm.

Q. Corrected Total Cell Fluorescence (CTCF) of Imp and Syp in WT and *lola*^{E76} clones at 72h ALH. n=8, 8, 8, and 8 clones.

R. Summary of *lola* loss-of-function phenotypes in the larval NE compared to WT and *nerfin-1* loss-of-function.

Data information: Data are represented as mean ± SEM. *p*-values were obtained using Mann-Whitney test and Wilcoxon matched-pairs signed rank test. ****$p < 0.0001$, ***$p < 0.001$, **$p < 0.005$, *$p < 0.05$

Lola but not Nerfin-1 promotes timely progression of the temporal series in the NE

Since Lola is expressed in the NE (Fig. 4H-I''') (35), we next investigated its function in this cell population. Our RNA-seq data showed that *Imp*, *mamo* and *Eip93F* expression levels were significantly altered in *lola*^{E76} compared to WT clones (Fig. S3H). In particular, *Imp* was upregulated (FC=79.5) whilst *mamo* and *Eip93F* were downregulated (FC=2.73 and 1.98, respectively). NE cells express a series of temporal factors consisted of Imp, Chinmo, Mamo, Syp, Br and Eip93F that are then inherited by their progenies (16) (Fig. 4L). Imp and Chinmo mark the early temporal window whilst Syp, Br, and Eip93F mark the late temporal window. In addition to our RNA-seq data, we performed immunostaining to examine the protein levels of Imp, Chinmo, Mamo and Syp in the medulla NE cells marked by DE-Cadherin (DE-Cad). At 72 hrs ALH (mid-L3), NE cells in WT clones expressed similar levels of Imp, Chinmo, Mamo, and Syp compared to their counterparts outside of the clones (Fig. 4M-M''', O-O'''). In contrast, *lola*^{E76} NE cells exhibited an upregulation of Imp and Chinmo as well as a downregulation of Mamo and Syp compared to NE cells outside of the clones (Fig. 4N-N''', P-P'''). Moreover, quantifications showed that Imp intensity in *lola*^{E76} NE cells was significantly higher compared to surrounding WT NE cells (internal control) and vice versa for Syp intensity (Fig. 4Q). Thus, our results suggest that the early temporal window in the NE was extended at the expense of the late temporal window upon Lola inactivation. Intriguingly, we also occasionally found that some *lola*^{E76} clones displayed a medially shifted NE/NB border at wandering L3 stage (Fig. S3I-I', arrowhead), indicative of a delayed NE-NB transition. As opposed to *lola*^{E76} clones, the expression of Imp,

412 Chinmo, Syp, and Mamo were not altered in *nerfin-1*^{159} NE cells compared to surrounding WT counterparts
413 (Fig. S3J-K'''). Altogether, our results suggest that only Lola, but not Nerfin-1 is required for the
414 progression of the temporal series in the NE (Fig. 4R).

415

416 **Chinmo and Imp promote the persistence of *lola*^{E76} dedifferentiated NBs in the pupal OL**

417 As Chinmo is the key determinant that sustains dedifferentiated NB proliferation during pupal life in *nerfin-*
418 *1*^{159} clones, we next examined Chinmo expression in *lola*^{E76} clones at wandering L3 stage in the OL. We
419 found that *lola*^{E76} clones expressed high levels of Chinmo (Fig. 5A-A''). To assess whether Chinmo
420 upregulation is functionally required to promote the persistence of *lola*^{E76} dedifferentiated NBs in the pupal
421 OL, we knocked down Chinmo in *lola*^{E76} clones by RNAi. This manipulation sufficiently reduced Chinmo
422 expression without significantly altering dedifferentiation in mutant clones at wandering L3 stage (Fig. 5A-
423 C). At 48 hrs APF, Chinmo knockdown caused a significant reduction in NB persistence in the OL, and a
424 dispersion of mutant cells, an indicator of neuronal differentiation (24) (Fig. 5D-E', G). In addition to
425 Chinmo, the RNA-binding protein Imp and Lin-28 are other components of the oncogenic module that
426 defines the oncogenic competency of dedifferentiated NBs in the VNC (26). In our RNA-seq data, we found
427 that differentially upregulated genes in *lola*^{E76} clones included both *Imp* and *lin-28* with FC of 79.5 and
428 2.41, respectively. Moreover, Imp knockdown in *lola*^{E76} clones was able to significantly reduce NB
429 persistence at 48 hrs APF, similar to Chinmo knockdown (Fig. 5D-G). Hence, Chinmo and Imp are required
430 to sustain *lola*^{E76} dedifferentiated NBs in the pupal OL.

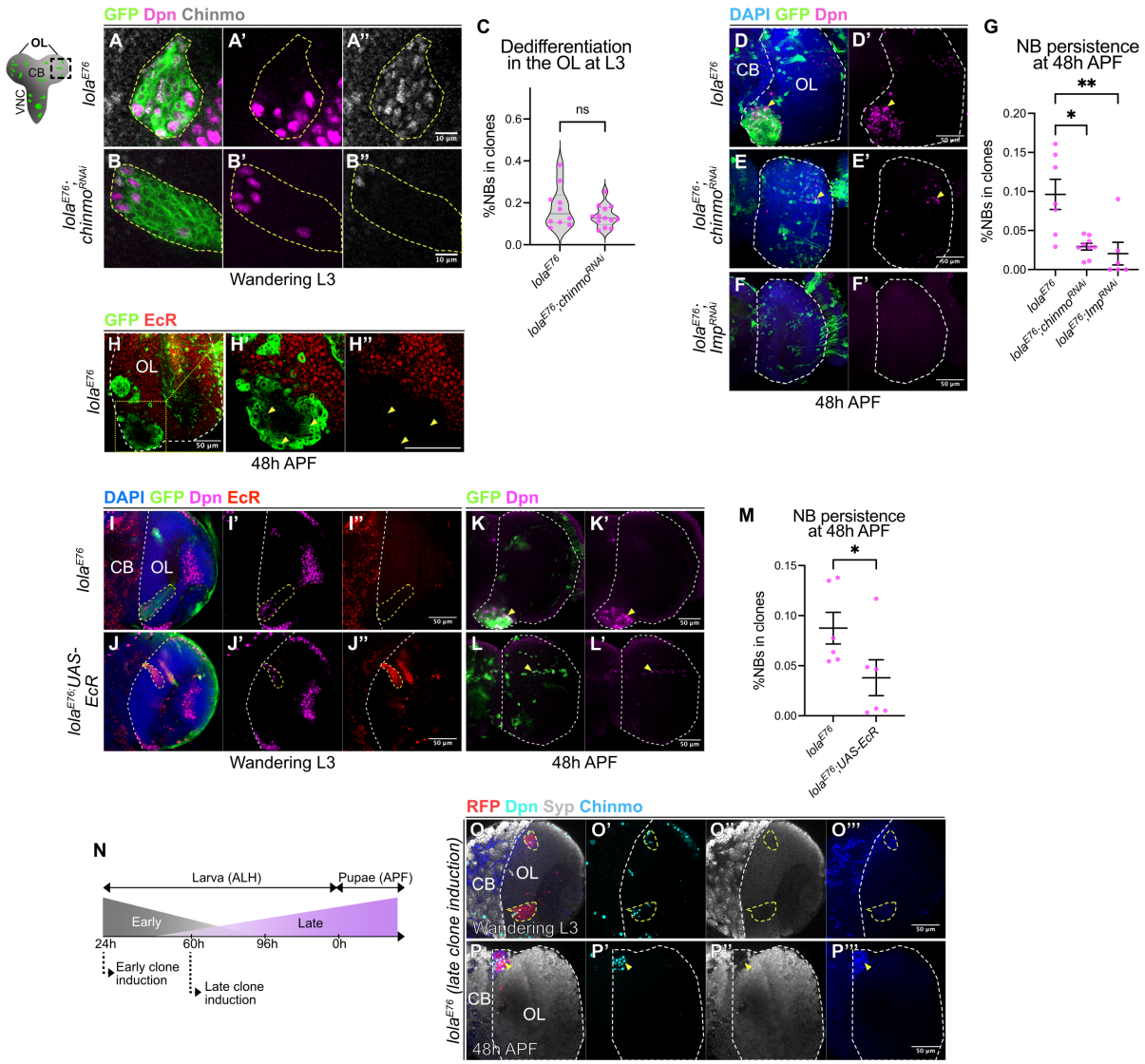

Figure 5: Chinmo and Imp promote the persistence of *lola*^{E76} NBs in the pupal OL

A-B". Single sections of **(A-A")** *lola*^{E76} and **(B-B")** *lola*^{E76}*;chinmo*^{RNAi} clones (dash lines) in the OLs (deep layer) at late L3. GFP (green), Dpn (magenta), Chinmo (grey). Scale bars: 10 µm.

C. NB percentages in *lola*^{E76} and *lola*^{E76}*;chinmo*^{RNAi} clones in the OLs at late L3. *lola*^{E76}: n=10 and 13 clones

D-F'. Maximum projections of the OLs (dash lines) at 48h APF with **(D)** *lola*^{E76}, **(E)** *lola*^{E76};*chinmo*^{RNAi} and **(F)** *lola*^{E76}*;Imp*^{RNAi} clones. Ectopic NBs (arrowheads). DAPI (blue), GFP (green), Dpn (magenta). Scale bars: 50 µm.

G. NB percentages in *lola*^{E76}, *lola*^{E76};*chinmo*^{RNAi}, and *lola*^{E76}*;Imp*^{RNAi} clones in the OLs at 48h APF. n=7, 9 and 6.

H-H". (H) Single section of the OL (dash lines) with *lola*^{E76} clones at 48h APF. **(H'-H")** Boxed areas in (H). Arrowheads indicate GFP^{+} cells. GFP (green), EcR (red). Scale bars: 50 µm.

I-J". Single section in the deep layers of the brain lobes at late L3 with **(I-I")** *lola*^{E76}, and **(J-J")** *lola*^{E76};*UAS-EcR* clones (yellow dash lines). DAPI (blue), GFP (green), Dpn (magenta), EcR (red). White dash lines indicate the CB/OL border. Scale bars: 50 µm.

K-L'. Single section of the OLs (dash lines) at 48h APF with **(K-K')** *lola*^{E76}, and **(L-L')** *lola*^{E76};*UAS-EcR* clones (arrowheads). GFP (green), Dpn (magenta). Scale bars: 50 µm.

M. NB percentages in *lola*^{E76} and *lola*^{E76};*UAS-EcR* clones in the OLs at 48h APF. n=6 and 6.

N. Clonal induction schematic.

O-O'''. Single section of the brain lobe (deep layer) with *lola*^{E76} clones (yellow dash lines) at late L3. RFP (red), Dpn (cyan), Syp (grey), Chinmo (blue). White dash lines indicate the CB/OL border. Scale bars: 50 µm.

P-P'''. Maximum projection of OL (dash lines) with *lola*^{E76} clones (arrowheads) at 48h APF. RFP (red), Dpn (cyan), Syp (grey), Chinmo (blue). Scale bars: 50 µm.

Data information: Data are represented as mean ± SEM. *p*-values were obtained using Mann-Whitney test and Kruskal-Wallis test with Dunn's test to correct for multiple comparisons. $^{**}p < 0.005$, $^{*}p < 0.05$

Chinmo upregulation occurs independently of ecdysone and the temporal identity of its cell of origin upon Lola inactivation

We next aimed to understand how Chinmo is regulated in *lola*^{E76} clones to sustain the proliferation of dedifferentiated NB in the pupal OL. As ecdysone signalling mediates the suppression of Chinmo to eliminate *nerfin-1*^{159}dedifferentiated NBs in the pupal OL, we wondered how *lola*^{E76} dedifferentiated NBs were able to retain Chinmo expression in spite of their location. Unlike *nerfin-1*^{159} clones that express EcR (Fig. 3L-L''), we found that EcR expression was downregulated in *lola*^{E76} clones compared to WT surrounding cells in the OL at 48 hrs APF (Fig. 5H-H'', arrowheads). As such, it is likely that *lola*^{E76} dedifferentiated NBs in the OL are not receptive to ecdysone signals that normally promote Chinmo silencing. To test if ecdysone signalling is sufficient to promote an elimination of *lola*^{E76} dedifferentiated NBs in the pupal OL, we overexpressed both isoforms A and B of EcR in *lola*^{E76} clones (Fig. 5I-J''). At 48 hrs APF, while *lola*^{E76} clones exhibited persistent ectopic NBs forming tumours in the OL, *lola*^{E76};*UAS-EcR* clones showed significantly less persistent NBs and the clones exhibited a dispersed morphology (Fig. 5K-M). Therefore, the absence of EcR in *lola*^{E76} clones facilitates the persistence of dedifferentiated NBs in the pupal OL.

We have shown that Lola promotes the progression of the early Imp^{+}Chinmo^{+} to late Syp^{+} temporal identity in the NE (Fig. 4R). In *lola*^{E76} clones, we observed that Chinmo was upregulated in the NBs on the superficial layers of the OL medulla at wandering L3 stage (Fig. S4A-A''' yellow arrowheads). This indicates that NBs and their progenies inherit the temporal identity of the NE cells in *lola*^{E76} clones. Thus, it is possible that *lola*^{E76} dedifferentiated NBs express Chinmo as they are generated during the Chinmo^{+}

478 time window (24 hrs ALH, early time point, Fig. 5N). To test this hypothesis, we induced *lola*^{E76} clones at
479 60 hrs ALH (late time point, Fig. 5N) to bypass the Chinmo^{+} time window. Despite being generated in the
480 Chinmo^{-} time window, *lola*^{E76} clones continued to express the early temporal marker Chinmo and failed to
481 turn on the late temporal marker Syp at wandering L3 stage (Fig. 5O-O'''). At 48 hrs APF, *lola*^{E76} ectopic
482 NBs were persistent in the OL (Fig. 5P-P'''). Thus, our data suggest that *lola*^{E76} dedifferentiated NBs can
483 persist independently of whether they are generated in the Chinmo^{+} or Chinmo^{-} temporal window.

484 Furthermore, we attempted to test if inhibiting the early temporal identity in the NE can prevent
485 the persistence of *lola*^{E76} dedifferentiated NBs in the pupal OL. To do so, we overexpressed Syp in *lola*^{E76}
486 clones, which was shown to repress the expression of Chinmo and Imp in the CB/VNC (Liu et al., 2015;
487 Ren et al., 2017; Yang et al., 2017). However, at 48 hrs APF, Syp overexpression was neither sufficient to
488 downregulate Imp, nor able to suppress the persistence of *lola*^{E76} ectopic NBs in the OL (Fig. S4B-D). Thus,
489 it is possible that the regulatory relationship between Imp-Chinmo-Syp in the OL may differ from that of
490 the CB/VNC.

491

492 **Notch signalling is not required for neuronal dedifferentiation in *lola*^{E76} clones**

493 We and others previously showed that neuronal dedifferentiation induced via *nerfin-1* loss-of-function in
494 the OL requires Notch signalling activation (19, 22). We wondered if Notch signalling is also required for
495 neuronal dedifferentiation induced by *lola* loss-of-function. Our RNA-seq data showed that while *Notch*
496 (*N*) was upregulated (FC=2.08) in *lola*^{E76} compared to WT cells, *Delta* which encodes for a Notch ligand,
497 as well as the downstream effector of Notch signalling, *E(spl)mγ* were not significantly altered (Fig. S4E).
498 In line with this, immunostaining in the OL showed that the intracellular domain of Notch (NICD) was
499 upregulated in *lola*^{E76} clones whereas Delta appeared not altered compared to WT cells surrounding the
500 clones at the wandering L3 stage (Fig. S4F-G''). To address if Notch signalling is necessary for neuronal
501 dedifferentiation induced by *lola* loss-of-function, we knocked down *N* via RNAi in *lola*^{E76} clones. This
502 manipulation did not significantly alter the rate of dedifferentiation at wandering L3 stage compared to the
503 *lola*^{E76} control (Fig. S4H-J). Together, our data suggest that Notch signalling does not mediate neuronal
504 dedifferentiation induced via Lola inactivation.

505

506 ***lola*^{E76} dedifferentiated NBs exhibited delayed temporal progression in the OL**

507 Medulla NBs sequentially express a series of tTFs including Homothorax (Hth), Eyeless (Ey), Sloppy
508 paired (Slp), Dichaete (D), and Tailless (Tll) as they age (36) (Fig. 6A). We next aimed to investigate

509 whether this temporal series is altered in *lola*^{E76} dedifferentiated NBs using three representative tTFs: the
510 early-tTF Ey, mid-tTF Slp and late-tTF Tll. It was previously shown that *lola* knockdown in medulla NBs
511 caused delayed temporal progression during late larval stages (35). Consistent with this, at wandering L3
512 stage, we observed that Ey, Slp, and Tll expression in *lola*^{E76} NBs appeared reduced compared to WT NBs
513 on the superficial layers, indicative of delayed temporal progression (Fig. 6B-F'''). Thus, our data confirms
514 the role of Lola in controlling the speed of temporal progression in the medulla NBs. In the deep layers of
515 the larval medulla where WT neurons and dedifferentiated NBs are located, we observed that a subset of
516 cells in *lola*^{E76} clones expressed Ey and Slp, but not Tll at wandering L3 stage (Fig. 6B, G-H'''). By 48 hrs
517 APF, fewer dedifferentiated NBs expressed Ey and Slp, and more cells expressed Tll in *lola*^{E76} clones (Fig.
518 6I-K). Together, our data suggest that *lola*^{E76} dedifferentiated NBs exhibited delayed progression through
519 the temporal series (Fig. 6L).

520 To test the requirement of tTF expression for *lola*-mediated dedifferentiation and tumorigenesis in
521 the OL, we manipulated three tTFs - Hth, Ey, and Slp in *lola*^{E76} clones. Upon the overexpression of Hth and
522 inhibition of Ey using validated fly lines (35, 37), we found that the rate of dedifferentiation was not
523 significantly altered compared to *lola*^{E76} control clones at wandering L3 stage (Fig. S5A-C', E). We also
524 knocked down Slp by *slp1*^{RNAi} (knockdown efficiency validated in fig. S5F-F'') in *lola*^{E76} clones. Similar to
525 Hth overexpression and Ey knockdown, Slp knockdown did not significantly alter the proportion of NBs
526 in *lola*^{E76} clones (Fig. S5D-E). Accordingly, our data suggest that the expression of these tTFs is dispensable
527 for the modulation of neuronal dedifferentiation caused by Lola inactivation. At 48 hrs APF, *lola*^{E76} clones
528 exhibited persistent NBs (Fig. S5G-G') and this phenotype was not significantly altered by the
529 manipulations of Hth, Ey and Slp (Fig. S5H-K). Taken together, our data suggest that although *lola*^{E76} NBs
530 display a delayed temporal progression from larval to pupal development, tTFs play minor roles in
531 promoting NB persistence and tumorigenesis in the OL.

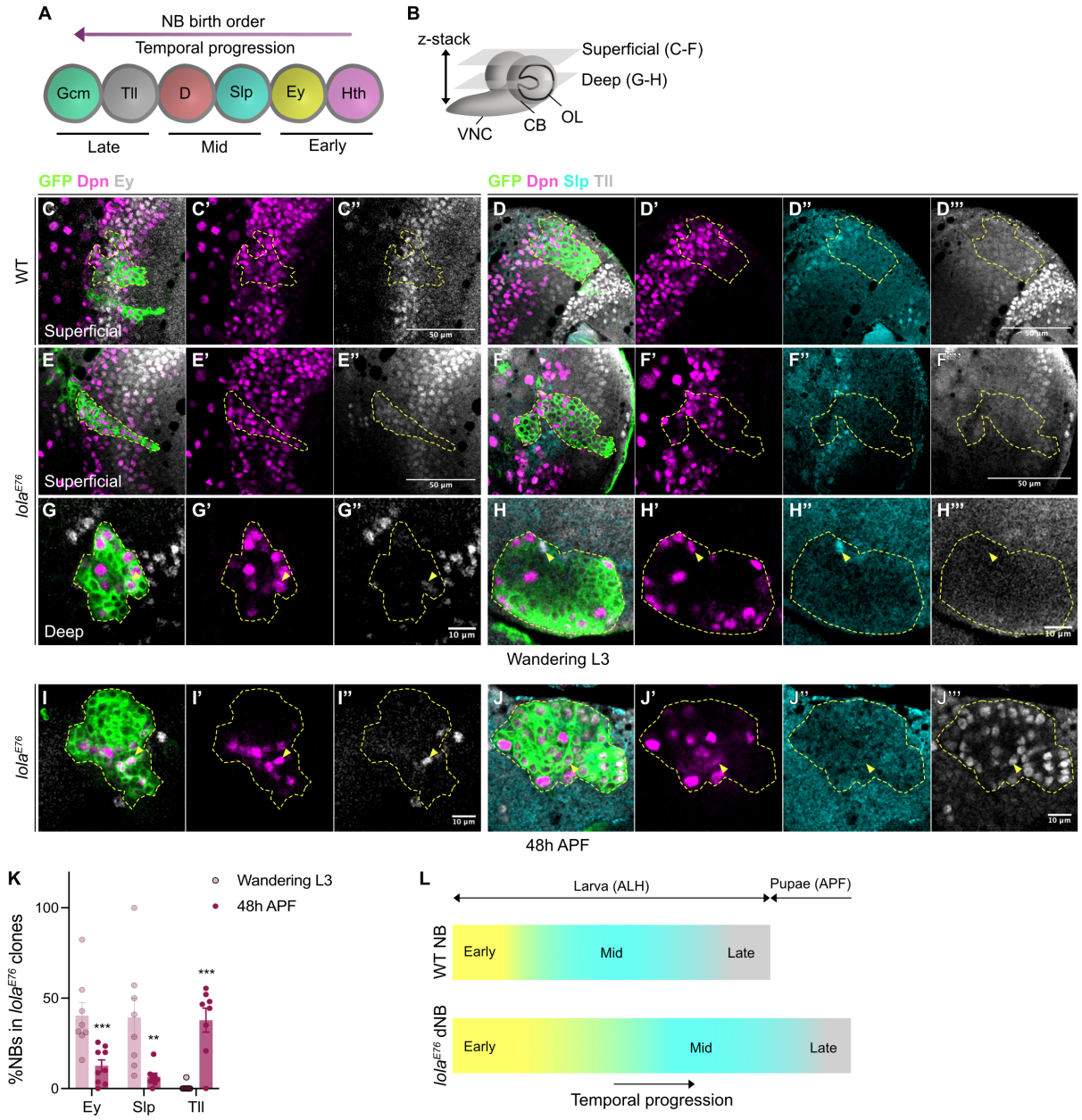

532

533 **Figure 6: Temporal progression is delayed in *lola*^{E76} dedifferentiated NBs**

534 **A.** Schematic depicting the temporal series in the medulla NBs.

535 **B.** Schematic depicting the side view of the larval CNS. Representative confocal images of the larval brain
536 are taken from either superficial (for Fig. 6C-F) or deep (for Fig. 6G-H) layers.

537 **C-F'''.** Single confocal sections of **(C-D''')** WT and (**E-F'''**) *lola*^{E76} clones (dash lines) on the superficial layers
538 of the medulla at wandering L3 stage. **(C-C'', E-E'')** GFP (green), Dpn (magenta), Ey (grey). **(D-D''', F-F''')**
539 GFP (green), Dpn (magenta), Slp (cyan), Tll (grey). Scale bars: 50 µm.

540 **G-H'''.** Single confocal sections of *lola*^{E76} clones (dash lines) in the deep layers of the medulla at wandering
541 L3 stage. **(G-G'')** GFP (green), Dpn (magenta), Ey (grey). Arrowheads indicate NBs expressing Ey. **(H-H''')**

542 GFP (green), Dpn (magenta), Slp (cyan), Tll (grey). Arrowheads indicate NBs expressing Slp. Scale bars:
543 10 μm.

544 **I-J'''.** Single confocal section of *lola*^{E76} clones (dash lines) in the OL at 48h APF. **(I-I'')** GFP (green), Dpn
545 (magenta), Ey (grey). Arrowheads indicate NBs expressing Ey. **(J-J''')** GFP (green), Dpn (magenta), Slp
546 (cyan), Tll (grey). Arrowheads indicate NBs expressing Tll. Scale bars: 10 μm.

547 **K.** Quantifications of the NB ratio expressing Ey, Slp, and Tll in *lola*^{E76} clones at wandering L3 stage and
548 48h APF in the OLs. n=8, 9, 8, 8, 8, and 8 clones.

549 **L.** Summary schematic depicting the delayed temporal progression in *lola*^{E76} dedifferentiated NBs (dNBs)
550 compared to WT NBs.

551 Data information: Data are represented as mean ± SEM. *p*-values were obtained using Multiple Mann-
552 Whitney test and Kruskal-Wallis test with Dunn's test to correct for multiple comparisons. ***$p < 0.001$,
553 **$p < 0.005$.

554

555 **Lola expression in *nerfin-1* loss-of-function clones promotes the elimination of dedifferentiated NBs**

556 Given that both Nerfin-1 and Lola are required to maintain the differentiated state of medulla neurons, we
557 wondered if these factors acted redundantly. To test this, we examined the expression of Lola.I::GFP
558 reporter in *nerfin-1*^{RNAi} flip-out clones at wandering L3 stage by immunostaining. We showed that Lola
559 expression was not altered in *nerfin-1*^{RNAi} clones compared to surrounding WT cells in the medulla (Fig.
560 7A-A'''). Similarly, *lola* mRNA expression level was comparable between *nerfin-1*^{159} and WT clones (Fig.
561 7B). To test if Lola is functionally required in *nerfin-1*^{159} dedifferentiated NBs, we knocked down Lola in
562 *nerfin-1*^{159} clones by RNAi. In *nerfin-1*^{159}, *lola*^{RNAi}, and *lola*^{RNAi}*;nerfin-1*^{159} clones, we observed ectopic NBs
563 in the deep layers of the medulla at wandering L3 stage (Fig. 1C, 7C-D'), indicative of neuronal
564 dedifferentiation. By 48 hrs APF, *lola*^{RNAi} *and lola*^{RNAi}*;nerfin-1*^{159} clones, but not *nerfin-1*^{159} clones displayed
565 persistent ectopic NBs in the OLs (Fig. 1M-M', 7E-F'). Notably, quantifications showed that NB
566 persistence in *lola*^{RNAi}*;nerfin-1*^{159} clones was significantly higher than that of *lola*^{RNAi} clones at 48 hrs APF
567 (Fig. 7G).

568 In the VNC, *lola*^{RNAi}*;nerfin-1*^{159} clones exhibited no significant difference in the percentages of NBs
569 at both wandering L3 stage and at 48 hrs APF (Fig. S6A-F), indicating that Lola is dispensable for *nerfin-*
570 *1* loss-of-function tumour overgrowth in this region. Collectively, our results suggest that Lola promotes
571 the elimination of dedifferentiated NBs in *nerfin-1* loss-of-function clones in the OL but not the CB/VNC
572 during pupal development.

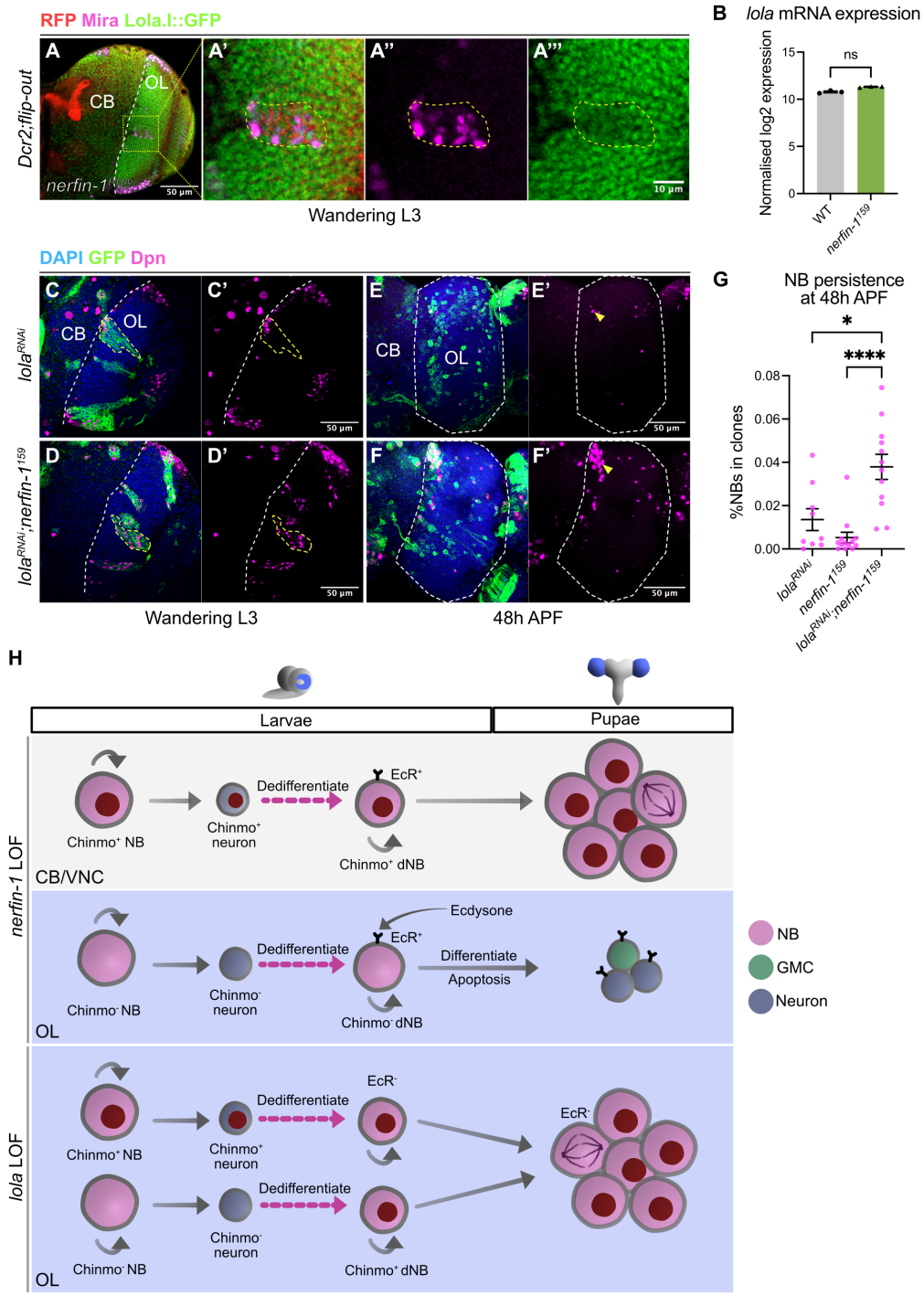

Figure 7: Lola expression in *nerfin-1* loss-of-function clones promotes elimination of ectopic NBs in the pupal OL

A-A'''. (A) Single confocal section in the deep layers of the brain lobe at wandering L3 stage with *nerfin-1*^{RNAi} flip-out clones. Scale bars: 50 µm. **(A'-A''')** is boxed area in (A). RFP (red), Mira (magenta). Scale bars: 10 µm. Lola.I::GFP (green). Yellow dash lines indicate mutant clones. White dash lines indicate the CB/OL borders.

580 **B.** *lola* normalised log2 expression from RNA-seq data of WT and *nerfin-1*^{159} cells collected from the late
581 larval OLs. n=3 and 3 samples.

582 **C-D'.** Single confocal sections in the deep layers of the brain lobes at wandering L3 stage with **(C-C')**
583 *lola*^{RNAi} and **(D-D')** *lola*^{RNAi};*nerfin-1*^{159} clones (yellow dash lines). DAPI (blue), GFP (green), Dpn (magenta).
584 White dash lines indicate the CB/OL borders. Scale bars: 50 µm.

585 **E-F'.** Maximum projections of the OLs (dash lines) at 48h APF with **(E-E')** *lola*^{RNAi} and **(F-F')** *lola*^{RNAi};*nerfin-*
586 *1*^{159} clones. DAPI (blue), GFP (green), Dpn (magenta). Arrowheads indicate ectopic NBs in the OLs. Scale
587 bars: 50 µm.

588 **G.** Quantifications of the NB percentages of *nerfin-1*^{159}, *lola*^{RNAi} and *lola*^{RNAi};*nerfin-1*^{159} clones in the OLs at
589 48h APF. n=13, 9 and 12.

590 **H.** Summary schematic: In the CB/VNC, Chinmo expression inherited from dedifferentiating *nerfin-1* loss-
591 of-function (LOF) neurons promotes persistence of dedifferentiated NBs (dNBs) during pupal stages. In the
592 OL, ecdysone signalling represses *chinmo* expression in *nerfin*-1 LOF clones, resulting in the elimination
593 of dNBs through terminal differentiation and apoptosis. *lola* LOF clones in the OL ectopically upregulates
594 Chinmo. Due to the absence of EcR in *lola* LOF clones, Chinmo expression is not suppressed, resulting in
595 dNB persistence in the pupal OL.

596 Data information: Data are represented as mean ± SEM. *p*-values were obtained using Mann-Whitney test
597 and Kruskal-Wallis test with Dunn's test to correct for multiple comparisons. ***$p < 0.001$, *$p < 0.05$.

598

599 **Discussion**

600 Dedifferentiation of mature specialised cells into stem-progenitor cells that can self-renew and re-
601 differentiate provides valuable opportunities for regeneration. However, studies have shown that
602 dedifferentiation can produce cancer stem cells that drive malignant tumour overgrowth and heterogeneity
603 (38). Thus, it is crucial to understand what factors determine these contrasting outcomes of
604 dedifferentiation. In this work, we have discovered that oncogenic tTFs are key determinants of this process.
605 In the CB/VNC, *nerfin-1*^{159} dedifferentiated NBs express the oncogenic tTF Chinmo that promotes their
606 persistence during pupal development. Conversely, in the OL, active ecdysone signalling promotes *chinmo*
607 silencing. The absence of Chinmo in turn enables the elimination of *nerfin-1*^{159} dedifferentiated NBs by
608 apoptosis and terminal differentiation. *lola*^{E76} dedifferentiated NBs on the other hand are not responsive to
609 ecdysone signals during pupal development, thereby ectopically express Chinmo and persist in the pupal
610 OL. Together, these mechanisms dictate the outcome of neuronal dedifferentiation (Fig. 7H). Our study
611 offers evidence that genetic mutations as well as region-specific cues can contribute to the oncogenic
612 competence of stem-progenitor cells derived from dedifferentiation.

613 **Chinmo is the key determinant of oncogenic competence in the CNS**

614 Our data suggest that the differential expression and regulatory mechanism of Chinmo can dictate the
615 oncogenic outcome of dedifferentiated NBs; such that high Chinmo induce oncogenesis whilst no/low
616 Chinmo allows elimination of the dedifferentiated progenitor pool. An outstanding question that remains to

617 be addressed is the mode-of-action of Chinmo. In the WT CB/VNC, Chinmo acts as a tTF that defines the
618 early temporal window in the NBs and their progenies, but not a regulator of NB proliferation (11, 26). In
619 *pros*$^{-/-}$ dedifferentiated tumours in the VNC, Chinmo was suggested to promote cell division and protein
620 synthesis (26). However, in the OL, Chinmo does not only act as a tTF in the NE progenitors and its progeny
621 but also governs NE cell self-renewal, and thereby, the timing of NE-NB transition (17). Therefore, whether
622 and how the function of Chinmo differs between the CB/VNC and the OL need further investigation.

623 **Steroid hormone signalling promotes elimination of dedifferentiated NBs by suppressing oncogenic**
624 **tTFs**

625 In the developing OL medulla, Chinmo expression is silenced in the NE by a pulse of ecdysone at critical
626 weight which coincides with the acceleration of the NE-NB transition, followed by post-embryonic
627 neurogenesis (17). As such, most medulla neurons are generated post-critical weight, during the Chinmo^{-}
628 time window and are thus incompetent to initiate tumour overgrowth following dedifferentiation. However,
629 because *nerfin-1*$^{-/-}$ clones were induced during the early Chinmo^{+} temporal window of the medulla, it was
630 unexpected that *nerfin-1*$^{-/-}$ dedifferentiated NBs did not inherit Chinmo expression. Our data showed that
631 *nerfin-1*$^{-/-}$ clones expressed EcR and thereby, are responsive to ecdysone signals between larval-pupal
632 development. This in turn promotes *chinmo* silencing, resulting in the elimination of dedifferentiated NBs.
633 Nevertheless, it remains to be addressed whether ecdysone signalling necessitates either or both the
634 initiation and the maintenance of Chinmo silencing in this case. In addition, how ecdysone signalling
635 controls Chinmo expression in the OL is yet to be interrogated. In the developing medulla, ecdysone
636 signalling at the mid-larval stage induces expression of its target gene *br* in the NE to promote the NE-NB
637 transition (18). In the wing imaginal disc, ecdysone signalling induces a Chinmo-to-Br expression switch
638 at the late larval stage (39). In addition, Br and Chinmo inhibit each other's expression (39, 40). As such, it
639 is possible that like the wing disc, ecdysone signalling inhibits Chinmo expression in the *nerfin-1*$^{-/-}$ clones
640 via its downstream effector Br. In *lola*$^{-/-}$ clones, despite their location in the OL, dedifferentiated NBs
641 continued to divide during late pupal stages (Fig. 4E-F). Unlike *nerfin-1*$^{-/-}$ clones, we found that *lola*$^{-/-}$ clones
642 did not express EcR and EcR misexpression is sufficient to eradicate *lola*$^{-/-}$ tumorigenesis in the pupal OL
643 (Fig. 5H-M). Nevertheless, further investigation is needed to better understand how Lola regulates EcR
644 expression. In the developing CB/VNC, it was previously shown that ecdysone signalling is dispensable
645 for Chinmo expression in the NBs (17), which may account for the persistence of the *nerfin-1*$^{-/-}$
646 dedifferentiated NBs in these regions.

647 **Lola regulates temporal progression in the medulla NE and dedifferentiated NBs**

648 We and other labs have shown that two Lola isoforms Lola.I and Lola.T are expressed in the larval NE (35)
649 (Fig. 4H-I'''). Here, our work has demonstrated that Lola regulates the progression of the early-to-late
650 temporal window in the NE progenitor pool. Intriguingly, some *lola*$^{-/-}$ clones exhibited a delayed NE-NB
651 transition (Fig. S3I-I'). Given that the expression of tTFs has been implicated in the regulation of NE self-
652 renewal and differentiation (17, 18), it is likely that Lola also governs the timing of the NE-NB transition
653 in the larval OL. As such, the previously demonstrated delay in temporal progression in the medulla NBs
654 upon Lola inactivation (35) might be a consequence of a delay in the NE-NB transition. Additionally, we
655 report that *lola*$^{-/-}$ dedifferentiated NBs exhibit delayed temporal progression (Fig. 6G-L). While it has been
656 suggested that the competence to generate brain tumours is determined by temporal identity (26, 41), our
657 results suggest that temporal progression of *lola*$^{-/-}$ dedifferentiated NBs plays a minor role in their
658 persistence and tumorigenicity (Fig. S5).

659 It is of note that we used *lola*^{E76} null mutation which removes all 12 Lola isoforms (34). This left
660 us unable to identify which Lola isoform functions in the NE, or to dissect the specific roles of each Lola
661 isoforms in different cell types (NE, NBs, neurons) in the medulla. Previous work showed that Lola-N
662 overexpression can rescue tumour overgrowth caused by *lola*^{E76} dedifferentiated NBs in the adult OL (20).
663 However, Lola-N mutant clones displayed no ectopic NBs in the adult OL (42), suggesting that there is
664 functional redundancy between Lola isoforms that needs to be taken into consideration.

665 **Differential target genes of Nerfin-1 and Lola in the developing medulla**

666 Our RNA-seq analyses have revealed that there is very little overlap between differential expressed genes
667 in *nerfin-1*$^{-/-}$ and *lola*$^{-/-}$ clones compared to the WT (Fig. S3E). This may account for the contrasting
668 tumorigenic phenotype between two mutations in the OL. The differentially expressed genes are enriched
669 in partially overlapping GO terms, in both cases, GO enrichment for downregulated genes involves
670 neuronal function and maturation (Fig. S3F-G). In *nerfin-1*$^{-/-}$, GO enrichment for upregulated genes
671 includes NB division and proliferation (Fig. S3G). This is expected given the expression pattern of Nerfin-
672 1 in immature neurons in the developing medulla (19, 22). Interestingly, GO enrichment for upregulated
673 genes in *lola*$^{-/-}$ clones are enriched in non-CNS genes (Fig. S3F). This echoes recent findings regarding the
674 chromatin remodeller Mi-2 and the condensin I subunit Cap-G whose knockdowns in neurons cause ectopic
675 upregulation of genes signatures of the fat body, the hindgut, or cilium assembly, etc, that tend to not
676 associate with the CNS (43, 44). Accordingly, it will be of interest to probe how Lola represses the
677 expression of organ and lineage inappropriate genes in the neurons, either via chromatin remodelling or
678 other mechanisms. A caveat in our study lies in transcriptomic profiling using bulk RNA-seq. As we have
679 demonstrated that Nerfin-1 and Lola are expressed and function differently in different cell types of the

680 developing medulla, it is unlikely that bulk RNA-seq precisely captured the gene network dynamic as well
681 as the heterogeneity of *nerfin-1*$^{-/-}$ and *lola*$^{-/-}$ clones.

682 Characterisations of paediatric brain tumours such as glioblastoma and medulloblastoma have
683 revealed the link between the oncogenic mutations, the tumour location and the overall prognosis in patients
684 (5–7). In glioblastoma, two mutations of the *H3F3* gene that lead to two amino acid substitutions of the
685 histone 3 variant 3, H3.3-G34R and H3.3-K27M induce tumour overgrowth in anatomical distinct regions
686 of the CNS. While the H3.3-G34R subtype is mostly found in the brain hemisphere, the H3.3-K27M
687 subtype is often found in the hindbrain (6, 7). A recent study using compartmentalised NSC culture derived
688 from anatomical relevant areas showed that high expression of the transcription factor FOXG1 in the
689 forebrain confers its housing NSCs the competency to undergo H3.3-G34R-induced oncogenic
690 transformation (45). Hence, differential gene expression profiles between brain regions appear to underpin
691 their varying susceptibility to oncogenic transformation. Our investigation further suggests that elucidating
692 the regionalised control of temporal patterning can aid us in understanding the outcome of dedifferentiated
693 tumours; however, the result needs to be considered within the context of a specific mutation.

694 **Materials and Methods**

695 **Fly stocks and husbandry**

696 The fly strains utilised are detailed Table 1.

697 **Table 1: Fly stock resources table**

System	Genotype	Source
Flip-out	*hs-FLP,act>CD2>GAL4;UAS-Dcr2,UAS-GFP*	Lei Zhang
	hsFLP; actc5>CD2>GAL4, UAS-GFP/TM6B	(21)
MARCM	*yw,hs-FLP;tub-GAL4,UAS-mCD8::GFP;FRT2A,tub-GAL80*	Alex Gould
	UAS-mCD8::GFP,hsFLP;FRT42D,tub-GAL80;tub-GAL4	Helena Richardson
	hs-FLP;FRT42D,tub-GAL80;tub-GAL4,UAS-mCD8::RFP	Kieran Harvey
	FRT42D,lola^{E76}	Tony Southall
	Df(3L)nerfin-1^{159}	Ward Odenwald
	FRT2A	Alex Gould
GAL4/GAL80	*ey^{R16F10}-GAL4*	BL48737
	tub-GAL80^{ts}	BL7108
Reporter	*Nerfin-1::GFP*	BL67385
	Lola.I::GFP	BL38662
	UAS-mCherry-chinmo^{UTRs}	Cedric Maurange
	chinmo-lacZ	BL10440
RNAi	*UAS-pros RNAi*	BL42538
	UAS-gcm RNAi	VDRC110539
	UAS-chinmo RNAi (III)	BL33638
	UAS-chinmo RNAi (II)	This study
	UAS-EcR^{DN}	BL9451
	UAS-Imp RNAi	BL34977
	UAS-nerfin-1 RNAi	VDRC101631
	UAS-lola RNAi	VDRC101925
	UAS-lola RNAi	BL26721
	UAS-mCherry RNAi	BL35784
	UAS-lacZ RNAi	Kieran Harvey
	UAS-ey RNAi	BL32486
	UAS-slp1 RNAi	BL29354
Overexpression	*UAS-p35*	BL5072
	UAS-Myc	BL9674
	UAS-chinmo^{FL}	BL50740
	UAS-syp^{RB}::HA	Tzumin Lee
	UAS-Imp.G	BL93386

	UAS-mCherry-let7^{Sponge}	BL61365
	UAS-EcR A+B	Leonie Quinn
	UAS-hth	BL98446
attP docking site	*P{CaryP}Msp300[attP40] (II)*	BL25709

698 Fly stocks were reared on standard media at 25ºC. For all experiments, embryos were collected overnight
699 at either room temperature or 25ºC. For larval dissection, brains were dissected at wandering L3 stage. For
700 pupal dissection, white pupae were selected and allowed to age to desired time points (24-48 hrs APF).

701 For clonal analysis, flip-out clones were induced at 24 hrs ALH, for 10 min at 37ºC then moved to
702 29ºC until dissection. This is except for experiments with *UAS-chinmo^{FL}* whereby clones were induced at
703 48 hrs ALH for 8 min and larva were allowed to develop until dissection at room temperature to prevent
704 animal lethality. Mosaic Analysis with a Repressible Cell Marker (MARCM) (46) clones were induced at
705 24 hrs ALH unless indicated otherwise, for 30 min at 37ºC and then moved to 29ºC until dissection. This
706 is except for experiments with *UAS-pros^{RNAi}* in which clones were induced for 15 min and animals were
707 kept at 25ºC to prevent excessive tumour overgrowth in the CNS.

708 For temporally restricted GAL4 expression by GAL80^{ts}, embryos were collected overnight at room
709 temperature and then moved to restrictive 18ºC for 5 days. Larva were next transferred to permissive 29ºC
710 to allow GAL4-induced transgene expression and dissected at either wandering L3 stage or 24 hrs APF.

711

712 **Generation of *UAS-chinmo^{RNAi}* (II) fly stock**

713 To generate *chimmo^{RNAi}* fly stock, oligos were designed based on the *UAS-chinmo^{RNAi}* TRiP line (BL33638),
714 with sense and anti-sense sequences as 5'-AGCGCGAATATCGTTGACAGA-3' and 5'-
715 TCTGTCAACGATATTCGCGCT-3', respectively. After annealing, the resulting DNA fragment was
716 cloned into VALIUM20 vector linearized by NheI and EcoRI. The ligation product was transformed into
717 Stable Competent *E.Coli* (NEB C3040H). Transformed colonies were selected by the presence of
718 pVALIUM20 vector by PCR with forward primer 5'-ACCAGCAACCAAGTAAATCAAC-3' and reverse
719 primer 5'-TAATCGTGTGTGATGCCTACC-3'. Plasmids were purified from selected colonies using
720 Isolate II Plasmid Miniprep (Meridian Bioscience) for sequencing and injected into flies carrying an attP40
721 docking site.

722

723 **Immunostaining**

724 Larval and pupal brains were dissected in phosphate buffered saline (PBS), fixed in 4% formaldehyde in
725 PBS for 20 min and rinsed three times in 0.5% Triton X-100 in PBS (PBST) at room temperature. For
726 immunostaining, brains were incubated in primary antibodies overnight at 4°C, followed by two 0.5% PBST
727 washes and then an overnight secondary antibody incubation at 4°C. Brains were next washed twice with
728 0.5% PBST and optically cleared in 50% glycerol for 20 min. Samples were mounted in either 80% glycerol
729 or anti-fade mounting medium containing 4% n-propyl gallate, on glass slides and sealed with coverslips
730 (22x22 mm, No 1.5) for image acquisition. The primary antibodies were: rat anti-Dpn (1:200, Abcam
731 195172), chick anti-GFP (1:1000, Abcam 13970), rat anti-Elav (1:50, DSHB 7E8A10), mouse anti-Repo
732 (1:50, DSHB 8D12), rabbit anti-Dcp-1 (1:100, Cell Signalling 95785), rabbit anti-Myc (1:100, Santa Cruz
733 Biotech d-1-717), rabbit anti-RFP (1:200, Rockland #600-401-379), mouse anti-Mira (1:100, a gift from
734 Alex Gould), rabbit anti-PatJ (1:500, a gift from Helena Richardson), rat anti-DE-Cad (1:200, DSHB
735 DCAD2), rat anti-Chinmo (a gift from Nicholas Sokol), guinea pig anti-Chinmo & rabbit anti-Syp & guine
736 pig anti-Mamo (1:200, gifts from Claude Desplan), mouse anti-EcR common (EcR^{comm}) (1:50, DSHB
737 Ag10.2), rabbit anti-Imp (1:500, a gift from Paul M Macdonald), mouse anti-NICD (1:50, DSHB C179C6),
738 mouse anti-Delta (1:10, DSHB C5949B), mouse anti-Ey (1:50, DSHB), guinea pig anti-Slp & rabbit anti-
739 Tll (1:200, gifts from Kuniaki Saito), Phalloidin 647 (1:10,000 Abcam 176759). Secondary donkey
740 antibodies conjugated to Alexa 555, Alexa 647, goat antibodies conjugated to Alexa 405, 488, 555, and 647
741 (Molecular Probes and Abcam) were used at 1:500.

742

743 **Image acquisition and processing**

744 Images were acquired using Olympus FV3000 confocal microscope with 40X (NA 0.95, UPSALO), and
745 60X (NA 1.30, UPLSAPO) objectives. Δz=1.5 µm. Images were processed using Fiji
746 (https://imagej.net/Fiji). Quantification was performed in Fiji or via 3D reconstruction in Imaris (Bitplane).
747 To quantify the percentages of NBs in clones at the larval stage or in the pupal OL in Imaris, GFP^+ volume
748 were first detected and measured. The GFP^+ volume were then utilised to make a mask for Dpn^+ cells which
749 was in turn used to measure the number of NB. The percentages of NBs in clones were calculated as the
750 number of GFP^+Dpn^+ cells/total GFP^+ volume x 100%. To quantify the percentages of neuron volume in
751 Imaris, GFP^+ volume in the whole OL or VNC were first detected and measured. The GFP^+ volume were
752 then utilised to make a mask for $Elav^+$ cells which was in turn used to measure total $Elav^+$ volume. The
753 percentages of neuron volume in clones were calculated as GFP^+Elav^+/total GFP^+ volume x 100%.
754 Quantifications of the percentages of NBs expressing tTFs (Ey, Slp, and Tll) in $lola^{E76}$ clones were done
755 manually in Fiji. Quantifications of the NB number in the OL at 24 hrs APF were done either manually in
756 Fiji or Imaris. Quantifications of Imp and Syp intensity in $lola^{E76}$ and WT cells around $lola^{E76}$ clones were

757 done in Fiji using Corrected Total Cell Fluorescence (CTCF) method. CTCF = Integrated Density – (Area
758 of selected cell x Mean fluorescence of background readings). Images were assembled in Affinity Publisher
759 2. Schematics were created in Affinity Design 2. Scale bars = 10, 20, or 50 μm per indicated.

760

761 **RNA-sequencing**

762 *FRT42D* (WT), *FRT2A,nerfin-1*^{159}, *FRT42D,lola*^{E76} mutant cells were isolated from wandering L3 stage
763 OLs by FACS purification using previously published protocol (47). Briefly, OLs were dissected from the
764 larval CNS in cold Schneider's culture medium (Gibco) and dissociated using papain and collagenase I
765 (Sigma-Aldrich). Cells were sorted by flow cytometry into lysis buffer and extracted for RNA using Single
766 cell purification kit (Norgen Biotek SKU51800). Samples from sorts executed on different days were
767 pooled into three samples per genotype, containing 33,000-105,000 cells (about 15-70 ng total RNA) per
768 sample. RNA concentration and quality were analysed by Tapestation Bioanalyzer 4150. Libraries were
769 amplified and prepared with QuantSeq (Lexogen) following standard protocol. RNA-sequencing was
770 carried out on NextSeq2000 instrument (Illumina), using 100 base single-end reads and 100 cycles. RNA-
771 seq samples consisted of three replicates per genotype and were all sequenced in the same batch.

772

773 **Bioinformatic analyses**

774 Alignment of the RNA-seq data to the *Drosophila melanogaster* reference genome (Release 6, Dm6) was
775 performed using Subread package. RNA-seq data analysis was performed according to a module designed
776 by COMBINE-Australia (Github: https://github.com/COMBINE-Australia/RNAseq-R) in RStudio.
777 FeatureCounts function in RSubread package was utilised to summarise reads into counts table in which
778 features mapped to multiple genes were excluded. edgeR and limma packages were employed to analyse
779 count data. To filter for lowly expressed genes, counts-per-million (CPM) were calculated and genes with
780 CPM<2 (equivalent to count<10) were discarded. To remove composition biases between libraries, TMM
781 normalisation was applied. To realise differential expression, counts data was transformed into $\log_2$CPM
782 using the voom function in the limma package. Individual gene expression is visualised as Normalised log2
783 expression i.e. $\log_2$CPM. The empirical Bayes method was used to perform empirical Bayes shrinkage on
784 the variances, estimate moderated t-statistics and generate p-values and $\log_2$(FC). To control for multiple
785 testing during exploratory analysis of our RNA-seq data, the testing relative to a threshold (treat) function
786 from the limma package was utilised to recalculate the moderated t-statistics and p-values for a FC cut-off
787 of 1.5 and p-value of 0.05. RNA-seq results were plotted in RStudio using gplots, ggplot2, and

788 VennDiagram packages. Perplexity AI (https://www.perplexity.ai/) was used to assist with R script
789 troubleshooting, taking error prompts as inputs.

790 Gene Ontology (GO) enrichment analyses were performed on gene symbols extracted from
791 org.Dm.eg.db package, using the topGO package in RStudio. Overrepresented GO terms were identified
792 through Fisher's exact test with weight method on genes with p-value<0.05 after treat. To realise GO
793 enrichment, differential expressed genes were compared with those of all known genes present in the
794 annotation. The results were plotted in RStudio using the ggplot2 package.

795

796 **Statistical analyses**

797 At least three animals per genotype were used for all experiments. Statistical analyses and plotting were
798 performed in GraphPad Prism 9. In graphs, data = mean ± standard error of the mean (SEM). n = lobes or
799 VNC unless specified. For comparisons between two conditions, p-values were calculated by non-
800 parametric Mann-Whitney tests when data show non-normally distribution. For comparisons between more
801 than two conditions, p-values were calculated by Kruskal-Wallis tests for non-normally distributed data.
802 Dunn's tests were used to correct for multiple comparisons following Kruskal-Wallis tests. For comparisons
803 of Imp and Syp intensities between $lola^{E76}$ and WT cells in the same brain, Wilcoxon matched-pairs signed
804 rank test were used. (*) $p<0.05$ (**) $p< 0.005$, (***) $p< 0.001$, (****) $p < 0.0001$, (ns) $p>0.05$.

Acknowledgements

We thank Lei Zhang, Helena Richardson, Kieran Harvey, Ward Odenwald, Alex Gould, Cedric Maurange, Tzumin Lee, Nicholas Sokol, Claude Desplan, Paul M Macdonald, Leonie Quinn and Kuniaki Saito for the generous sharing of antibodies and fly stocks. We thank Qian Dong for critical reading of the manuscript; Abdul Jabbar Saiful Hilmi and Sofya Golenkina for assisting with the generation of *UAS-chinmo*^{RNAi} construct; Katrina Mitchell for assisting with RNA-seq data analyses; Perplexity AI for R script troubleshooting. We thank the Bloomington *Drosophil*a Stock Centre (BDSC), Vienna *Drosophila* Resource Centre (VDRC), and Developmental Studies Hybridoma Bank (DSHB) for fly stocks and antibodies. We thank OZDros for *Drosophila* quarantine. We thank Centre for Advanced Histology and Microscopy (RRID:SCR_025432), Research Flow Core (RRID:SCR_025550), and Molecular Genomics Core (RRID:SCR_025695) at Peter MacCallum Cancer Centre for access and support. We thank Australian *Drosophila* Transgenic Facility for injection service.

Funding

PKN is funded by a PhD scholarship from the Department of Anatomy and Physiology, Faculty of Medicine, Dentistry and Health Sciences, The University of Melbourne and the Vingroup Science and Technology Scholarship Program for Overseas Study for Master's and Doctoral Degrees. LYC's laboratory is supported by funding from the NHMRC Ideas Grant (APP2011289).

Author contributions

PKN: Writing - original draft, Conceptualization, Investigation, Writing - review & editing, Methodology, Resources, Data curation, Validation, Formal analysis, Software, Visualization.

FF: Conceptualization, Methodology, Validation.

OM: Methodology.

TS: Methodology.

LYC: Writing-original draft, Conceptualization, Investigation, Writing - review & editing, Methodology, Resources, Funding acquisition, Data curation, Validation, Supervision, Formal analysis, Project administration, Visualization.

Disclosure and competing interests statement

The authors declare they have no competing interest.

Data availability

All data needed to evaluate the conclusions in the paper are present in the paper. The *UAS-chinmo*^{RNAi} (II) *Drosophila* stock can be provided by Louise Y Cheng. Requests for this *Drosophila* stock should be submitted to louise.cheng@petermac.org. RNA-seq produced in this study is available at GEO (accession number: GSE306602).

842 **References**

843 1. L. Pavinato, A. Baggiolini, Oncogenic competence: balancing mutations, cellular state, and
844 microenvironment. *Trends in Cancer* (2025). https://doi.org/10.1016/j.trecan.2025.01.002.

845 2. M. Bruschi, J. Grill, L. Guerrini-Rousseau, Pediatric brain tumors as a developmental disease.
846 *Current Opinion in Oncology* **33**, 608–614 (2021).

847 3. G. M. Marshall, *et al.*, The prenatal origins of cancer. *Nat Rev Cancer* **14**, 277–289 (2014).

848 4. X. Chen, W. Yang, C. W. M. Roberts, J. Zhang, Developmental origins shape the paediatric cancer
849 genome. *Nat Rev Cancer* **24**, 382–398 (2024).

850 5. P. Gibson, *et al.*, Subtypes of medulloblastoma have distinct developmental origins. *Nature* **468**,
851 1095–1099 (2010).

852 6. A. Mackay, *et al.*, Integrated Molecular Meta-Analysis of 1,000 Pediatric High-Grade and Diffuse
853 Intrinsic Pontine Glioma. *Cancer Cell* **32**, 520-537.e5 (2017).

854 7. D. Sturm, *et al.*, Hotspot Mutations in H3F3A and IDH1 Define Distinct Epigenetic and Biological
855 Subgroups of Glioblastoma. *Cancer Cell* **22**, 425–437 (2012).

856 8. A. Hofbauer, J. A. Campos-Ortega, Proliferation pattern and early differentiation of the optic lobes
857 in Drosophila melanogaster. *Rouxs Arch Dev Biol* **198**, 264–274 (1990).

858 9. K. Ito, Y. Hotta, Proliferation pattern of postembryonic neuroblasts in the brain of Drosophila
859 melanogaster. *Developmental Biology* **149**, 134–148 (1992).

860 10. J. W. Truman, M. Bate, Spatial and temporal patterns of neurogenesis in the central nervous system
861 of Drosophila melanogaster. *Developmental Biology* **125**, 145–157 (1988).

862 11. C. Maurange, L. Cheng, A. P. Gould, Temporal transcription factors and their targets schedule the
863 end of neural proliferation in Drosophila. *Cell* **133**, 891–902 (2008).

864 12. P.-K. Nguyen, L. Y. Cheng, Drosophila medulla neuroblast termination via apoptosis,
865 differentiation, and gliogenic switch is scheduled by the depletion of the neuroepithelial stem cell
866 pool. *eLife* **13**, e96876 (2024).

867 13. Q. Ren, *et al.*, Stem Cell-Intrinsic, Seven-up-Triggered Temporal Factor Gradients Diversify
868 Intermediate Neural Progenitors. *Current Biology* **27**, 1303–1313 (2017).

869 14. M. H. Syed, B. Mark, C. Q. Doe, Steroid hormone induction of temporal gene expression in
870 Drosophila brain neuroblasts generates neuronal and glial diversity. *eLife* **6**, e26287 (2017).

871 15. C.-P. Yang, *et al.*, Imp and Syp RNA-binding proteins govern decommissioning of Drosophila
872 neural stem cells. *Development* **144**, 3454–3464 (2017).

873 16. U. Arain, I. M. Islam, P. Valentino, T. Erclik, Concurrent temporal patterning of neural stem cells in
874 the fly visual system. [Preprint] (2022). Available at:
875 https://www.biorxiv.org/content/10.1101/2022.10.13.512100v1 [Accessed 20 December 2024].

876 17. C. Dillard, K. Narbonne-Reveau, S. Foppolo, E. Lanet, C. Maurange, Two distinct mechanisms
877 silence chinmo in Drosophila neuroblasts and neuroepithelial cells to limit their self-renewal.
878 *Development* **145** (2018).

879 18. Y. Zhou, *et al.*, Broad Promotes Neuroepithelial Stem Cell Differentiation in the Drosophila Optic
880 Lobe. *Genetics* **213**, 941–951 (2019).

881 19. J. Xu, *et al.*, Prevention of medulla neuron dedifferentiation by Nerfin-1 requires inhibition of Notch
882 activity. *Development* **144**, 1510–1517 (2017).

883 20. T. D. Southall, C. M. Davidson, C. Miller, A. Carr, A. H. Brand, Dedifferentiation of Neurons
884 Precedes Tumor Formation in lola Mutants. *Developmental Cell* **28**, 685 (2014).

885 21. F. Froldi, *et al.*, The transcription factor Nerfin-1 prevents reversion of neurons into neural stem
886 cells. *Genes Dev.* **29**, 129–143 (2015).

887 22. J. H. A. Vissers, *et al.*, The Scalloped and Nerfin-1 Transcription Factors Cooperate to Maintain
888 Neuronal Cell Fate. *Cell Reports* **25**, 1561-1576.e7 (2018).

889 23. A. Kuzin, T. Brody, A. W. Moore, W. F. Odenwald, Nerfin-1 is required for early axon guidance
890 decisions in the developing *Drosophila* CNS. *Developmental Biology* **277**, 347–365 (2005).

891 24. J. Morante, T. Erclik, C. Desplan, Cell migration in Drosophila optic lobe neurons is controlled by
892 eyeless/Pax6. *Development (Cambridge, England)* **138**, 687 (2011).

893 25. S. Genovese, *et al.*, Coopted temporal patterning governs cellular hierarchy, heterogeneity and
894 metabolism in Drosophila neuroblast tumors. *eLife* **8**, e50375 (2019).

895 26. K. Narbonne-Reveau, *et al.*, Neural stem cell-encoded temporal patterning delineates an early
896 window of malignant susceptibility in Drosophila. *eLife* **5**, e13463 (2016).

897 27. S. Zhu, *et al.*, Gradients of the Drosophila Chinmo BTB-Zinc Finger Protein Govern Neuronal
898 Temporal Identity. *Cell* **127**, 409–422 (2006).

899 28. B. Egger, J. Q. Boone, N. R. Stevens, A. H. Brand, C. Q. Doe, Regulation of spindle orientation and
900 neural stem cell fate in the Drosophila optic lobe. *Neural Dev* **2**, 1 (2007).

901 29. T. Yasugi, D. Umetsu, S. Murakami, M. Sato, T. Tabata, Drosophila optic lobe neuroblasts triggered
902 by a wave of proneural gene expression that is negatively regulated by JAK/STAT. *Development*
903 **135**, 1471–1480 (2008).

904 30. C. S. Thummel, Molecular Mechanisms of Developmental Timing in *C. elegans* and *Drosophila*.
905 *Developmental Cell* **1**, 453–465 (2001).

906 31. M. H. Sieber, A. C. Spradling, Steroid Signaling Establishes a Female Metabolic State and
907 Regulates SREBP to Control Oocyte Lipid Accumulation. *Current Biology* **25**, 993–1004 (2015).

908 32. Z. Liu, *et al.*, Opposing intrinsic temporal gradients guide neural stem cell production of varied
909 neuronal fates. *Science* **350**, 317–320 (2015).

910 33. Y. Jiang, M. Seimiya, T. B. Schlumpf, R. Paro, An intrinsic tumour eviction mechanism in
911 Drosophila mediated by steroid hormone signalling. *Nat Commun* **9**, 3293 (2018).

912 34. S. Goeke, *et al.*, Alternative splicing of lola generates 19 transcription factors controlling axon
913 guidance in Drosophila. *Nat Neurosci* **6**, 917–924 (2003).

914 35. H. Zhu, S. D. Zhao, A. Ray, Y. Zhang, X. Li, A comprehensive temporal patterning gene network in
915 Drosophila medulla neuroblasts revealed by single-cell RNA sequencing. *Nat Commun* **13**, 1247
916 (2022).

917 36. X. Li, *et al.*, Temporal patterning of Drosophila medulla neuroblasts controls neural fates. *Nature*
918 **498**, 456–462 (2013).

919 37. C.-Y. Pai, *et al.*, The Homothorax homeoprotein activates the nuclear localization of another
920 homeoprotein, Extradenticle, and suppresses eye development in Drosophila. *Genes Dev* **12**, 435–
921 446 (1998).

922 38. D. Friedmann-Morvinski, I. M. Verma, Dedifferentiation and reprogramming: origins of cancer
923 stem cells. *EMBO reports* **15**, 244–253 (2014).

924 39. K. Narbonne-Reveau, C. Maurange, Developmental regulation of regenerative potential in
925 Drosophila by ecdysone through a bistable loop of ZBTB transcription factors. *PLOS Biology* **17**,
926 e3000149 (2019).

927 40. S. Chafino, P. Giannios, J. Casanova, D. Martín, X. Franch-Marro, Antagonistic role of the BTB-
928 zinc finger transcription factors Chinmo and Broad-Complex in the juvenile/pupal transition and in
929 growth control. *eLife* **12**, e84648 (2023).

930 41. D. R. Farnsworth, O. A. Bayraktar, C. Q. Doe, Aging Neural Progenitors Lose Competence to
931 Respond to Mitogenic Notch Signaling. *Current Biology* **25**, 3058–3068 (2015).

932 42. N. Dinges, V. Morin, N. Kreim, T. D. Southall, J.-Y. Roignant, Comprehensive Characterization of
933 the Complex *lola* Locus Reveals a Novel Role in the Octopaminergic Pathway via Tyramine Beta-
934 Hydroxylase Regulation. *Cell Reports* **21**, 2911–2925 (2017).

935 43. G. N. Aughey, E. Forsberg, K. Grimes, S. Zhang, T. D. Southall, NuRD-independent Mi-2 activity
936 represses ectopic gene expression during neuronal maturation. *EMBO reports* **24**, e55362 (2023).

937 44. A. Hassan, *et al.*, Condensin I subunit Cap-G is essential for proper gene expression during the
938 maturation of post-mitotic neurons. *eLife* **9**, e55159 (2020).

939 45. R. B. Bressan, *et al.*, Regional identity of human neural stem cells determines oncogenic responses
940 to histone H3.3 mutants. *Cell Stem Cell* **28**, 877-893.e9 (2021).

941 46. T. Lee, L. Luo, Mosaic Analysis with a Repressible Cell Marker for Studies of Gene Function in
942 Neuronal Morphogenesis. *Neuron* **22**, 451–461 (1999).

943 47. H. Harzer, C. Berger, R. Conder, G. Schmauss, J. A. Knoblich, FACS purification of Drosophila
944 larval neuroblasts for next-generation sequencing. *Nat Protoc* **8**, 1088–1099 (2013).

945